

Characterisation of Performance of Thin-film Photovoltaic Technologies



PVPS

PHOTOVOLTAIC
POWER SYSTEMS
PROGRAMME

Report IEA-PVPS T13-02:2014

*Outdoor test facility for the comparison of energy yield measurements of different photovoltaic module technologies.
Courtesy of TÜV Rheinland, Energie und Umwelt GmbH, Cologne, Germany.*

INTERNATIONAL ENERGY AGENCY
PHOTOVOLTAIC POWER SYSTEMS PROGRAMME

Characterisation of Performance of Thin-film Photovoltaic Technologies

IEA PVPS Task 13, Subtask 3.1
Final Report IEA-PVPS T13-02:2014
May 2014

ISBN 978-3-906042-17-6

Authors:

Timothy J Silverman
National Renewable Energy Laboratory, Golden, CO, USA

Ulrike Jahn
TÜV Rheinland Energie und Umwelt GmbH, Cologne, Germany

Gabi Friesen and Mauro Pravettoni
SUPSI ISAAC, Canobbio, Switzerland

Marco Apolloni
TEL Solar, Trübbach, Switzerland

A Louwen and WGJHM van Sark
Utrecht University, Copernicus Institute of Sustainable
Development, Utrecht, the Netherlands

Markus Schweiger
TÜV Rheinland Energie und Umwelt GmbH, Cologne, Germany

G. Belluardo, J. Wagner, A. Tetzlaff, P. Ingenhoven, D. Moser
EURAC Research Institute for Renewable Energy, Bolzano, Italy

Further contributions and data from:

Anne Gerd Imenes, Teknova, Norway
Lionel Sicot, Guillaume Razongles, CEA INES, France
Tom Betts, CREST, United Kingdom
George E. Georghiou, University of Cyprus
Mike van Iseghem, Didier Binesti, EDF R&D, France

This report is supported by:

Austrian Federal Ministry for Transport, Innovation and Technology (BMVIT) under FFG
contract No. 828105

German Federal Ministry for Economic Affairs and Energy under Contract No.0325194A
(BMWi)

Supported by:



on the basis of a decision
by the German Bundestag

Swiss Federal Office of Energy (SFOE)

“FLASH”, a *Perspectief* programme funded by Technology Foundation STW (<http://stw.nl/en/>)
under project number 12172

and

U.S. Department of Energy under Contract No. DE-AC36-08-GO28308 with the National
Renewable Energy Laboratory (NREL)

Table of Contents

1	Foreword.....	1
2	Executive Summary	2
3	Simulator Performance.....	3
	3.1 Previous work	3
	3.1.1 Introduction.....	3
	3.1.2 State of the art in indoor performance characterization of PV modules with solar simulators.....	3
	3.1.3 Specific issues in thin-film modules.....	7
	3.1.4 References for this section	10
	3.2 Stabilisation issues particular to thin-film PV modules	11
	3.2.1 Introduction.....	11
	3.2.2 Recent results in thin-film stabilisation	11
	3.2.3 Improving upon thin-film PV stabilisation methods	16
	3.3 Performance characterization of thin-film multi-junction PV cells and modules	22
	3.3.1 Introduction.....	22
	3.3.2 Theory and definitions.....	22
	3.3.3 Basics of measurement methods	24
	3.3.4 Acknowledgments.....	29
	3.3.5 References for this section	30
4	Field performance	32
	4.1 Introduction	32
	4.2 Summary of previous studies in the literature.....	32
	4.2.1 Introduction.....	32
	4.2.2 Spectral effects.....	32
	4.2.3 Temperature effects.....	34
	4.2.4 Transient and seasonal performance changes	35
	4.2.5 References for this section	37
	4.3 Comparison of Different PV Module Technologies: New Method to Analyse Performance Characteristics Obtained from Field Tests at Different Locations	38
	4.3.1 Motivation	38
	4.3.2 Approach	38
	4.3.3 Results	40
	4.3.4 References for this section	44
	4.4 Analysis of spectral effects on outdoor performance	44
	4.4.1 Spectral response measurements	44
	4.4.2 Measuring solar spectral irradiance	45
	4.4.3 Analysis of large amounts of spectral data with the APE factor	47
	4.4.4 Correlating SR data and spectral data with module performance.....	49
	4.4.5 Influence of spectral effects on the energy yield of single-junction modules.....	50
	4.4.6 References for this section	51
	4.5 Modeled spectrum method.....	51
	4.5.1 Introduction.....	51
	4.5.2 Description of methodology	51
	4.5.3 Results	53
	4.5.4 Acknowledgements.....	57
	4.5.5 References for this section	57

List of Figures

Fig. 1: Spread of P_{max} at STC (deviation from average of six test laboratories) as measured with different solar simulators and four different crystalline silicon module types	4
Fig. 2: Spread of P_{max} at 200 W/m ² (deviation from average of six test laboratories) as measured with different solar simulators and four different crystalline silicon module types	5
Fig. 3: Spread of P_{max} temperature coefficient measured at 800 W/m ² (deviation from average of six test laboratories) as measured with different solar simulators and four different crystalline silicon module types.	5
Fig. 4: Spread of P_{max} at STC (deviation from average of six test laboratories) as measured with different solar simulators and four different thin-film module technologies within the second round-robin	6
Fig. 5: Normalised PV parameters of single junction thin-film devices as measured (i) outdoors, (ii) indoors without spectral mismatch correction, and (iii) indoors with spectral mismatch correction. The variations are relative to the outdoor measurement [21].	9
Fig. 6: Normalised power (P_{max}) of single-junction thin-film devices (left) and double-junction and hybrid a-Si (right) module, measured as a function of I-V sweep-time. The dashed line indicates a typical sweep-time used for the LAPSS solar simulator [21].....	9
Fig. 7: Electrical stabilisation of a CIGS specimen during light-soaking at 1000 W/m ² and a module temperature of 58.4°C	12
Fig. 8: Irreversible degradation of a CIGS specimen caused by light-soaking at 83.7°C module temperature, online-monitored module parameters at 1000 W/m ²	12
Fig. 9: Electrical stabilisation of a CdTe specimen during light-soaking at 1000 W/m ² at a module temperature of 79.4°C	13
Fig. 10: Stabilisation of a CdTe specimen during light-soaking at 26.8°C module temperature and 1000 W/m ²	14
Fig. 11: Relative change of the nominal power of CIGS specimens during dark storage at various temperatures	15
Fig. 12: Relative change of the nominal power of CdTe specimens during dark storage at various temperatures	15
Fig. 13: Metastable evolution of the current-voltage characteristic measured for a CdTe module upon light exposure	16
Fig. 14: Open circuit voltage (V_{oc}), fill factor (FF) and maximum power (P_{max}) of a commercial CdTe module depending on light exposure time and electrical bias	17
Fig. 15: Pairs of modules were repeatedly characterised after stabilisation by light-soaking. Between measurements, modules were stored in the dark unbiased (left) and biased at I_{mp} (right).	20
Fig. 16: Two modules were continuously measured upon outdoor exposure after unbiased dark storage (black points) and biased at $I(V_{mp})$ (red points). P_{max} is shown normalised to the final power and corrected for module back temperature and irradiance. [11].	21
Fig. 17: Single and multi-junction PV devices compared to conventional voltage generators [3].	23
Fig. 18: SR measurement setup, based on: (a) lock-in technique; (b) a filtered pulsed simulator. The shunt resistor may be replaced by a trans-impedance amplifier (TIA) [28].	28
Fig. 19: Spectral response of different module types (CIS, a-Si, c-Si) [4].	33

Fig. 20: Modelled dependence of I_{sc} on Air Mass of incident radiation, for single junction a-Si (blue circles) and crystalline silicon (red squares). The dark lines are linear fits to the modeled data points [6].	34
Fig. 21: Left: Overview of the seasonal effects of temperature (ϵ_t), SWE (ϵ_{swe}), reflection (ϵ_r) and spectrum (ϵ_s) on a-Si performance. The effects are expressed as performance factors, the ratio of actual vs. rated performance due to each factor. The total performance factor is obtained by multiplication of the four individual performance factors [5]. Right: Seasonal changes of selected amorphous silicon devices [19].	36
Fig. 22: Monthly average DC performance ratio for thin-film CIGS and CdTe systems over the period June 2006 – June 2010 in Nicosia, Cyprus [14].	36
Fig. 23: Meteorological data during monitoring period 2010-2012 at seven different sites. The upper figure shows the different distributions of daily irradiation sums, the lower figure shows the monthly average ambient temperatures measured at the sites.	39
Fig. 24: Average back-of-module temperature for irradiances $G > 0 \text{ W/m}^2$ (line plots) and daily PR for P_{max} (dot plots) for <i>c-Si modules</i> at five different sites during monitoring period May 2010 to Dec 2012.	40
Fig. 25: Example of analysis approach with daily performance ratio $PR(P_{max})$ (top/right) and $PR(I_{sc})$ (top/left) of 6 different <i>c-Si modules</i> measured at different locations. Step 1: merge to normalised performance ratio norm. $PR(P_{max})$ and Step 2: plot in dependence of daily irradiation (bottom/left) and of average daylight module temperature (bottom/right).	41
Fig. 26: Average back-of-module temperature for irradiances $G > 0 \text{ W/m}^2$ (line plots) and daily PR of P_{max} (dot plots) for <i>a-Si based modules</i> measured in different locations during monitoring period May 2010 to Dec 2012.	42
Fig. 27: Example of analysis approach with daily performance ratio $PR(P_{max})$ (top/right) and $PR(I_{sc})$ (top/left) of 7 different <i>a-Si based silicon modules</i> measured in different locations. Step 1: merge to normalised performance ratio norm $PR(P_{max})$ and Step 2: plot in dependence of daily irradiation (bottom/left) and of average daylight module temperature (bottom/right).	43
Fig. 28: Relative spectral response signal of different modules, illustrating significant differences within the same thin-film technology.	45
Fig. 29: Angular characteristic of the best performing input optic: spectrally neutral but increasing cosine error above 40° .	46
Fig. 30: Angular characteristic of the worst performing input optic: wavelength dependent cosine error.	46
Fig. 31: Solar spectral irradiance drift for four cloudless days in summer (red), spring (orange), all (yellow) and winter (blue), mounted facing south and tilted 35° , in Cologne.	48
Fig. 32: Characterization of a partly cloudy day (29.08.2010) and correlation of APE values with the appearance of clouds.	48
Fig. 33: Seasonal variations of APE values and average APE value per month.	49
Fig. 34: Dependence of measured I_{sc} on spectral changes (T, G corrected, normalised to $I_{sc, STC}$ (=100%) at 1.65 eV).	50
Fig. 35: Average spectrum of the period 01.09.11–31.08.12 relative to AM1.5, area normalised.	50
Fig. 36: Comparison of horizontal simulated and measured irradiance for ABD test installation, year 2011. Top: unfiltered points (RMSE=80.2). Bottom: clear sky conditions (RMSE=31.8).	53

Fig. 37: Comparison of in-plane simulated and measured irradiance for ABD test installation, year 2011. Top: unfiltered points (RMSE=100.870). Bottom: clear sky conditions (RMSE=71.264) 54

Fig. 38: Normalised efficiency against average wavelength, for clear sky conditions, angle of incidence less than 50°, sorted for shading (left) and filtered and corrected for standard temperature of 25°C (right). Different in-plane irradiance levels are displayed. 57

List of Tables

Tab. 1: State-of-the-art efficiencies for various single- and multi-junction technologies, compared with the c-Si record device and with the III-V multi-junction record cell. All records refer to 1000 W/m², AM1.5g spectrum and 25°C cell temperature [4-5]. 24

Tab. 2: Parameters defined and used to perform common data analysis 39

1 Foreword

The International Energy Agency (IEA), founded in November 1974, is an autonomous body within the framework of the Organization for Economic Co-operation and Development (OECD) which carries out a comprehensive programme of energy co-operation among its member countries. The European Union also participates in the work of the IEA. Collaboration in research, development and demonstration of new technologies has been an important part of the Agency's Programme.

The IEA Photovoltaic Power Systems Programme (PVPS) is one of the collaborative R&D Agreements established within the IEA. Since 1993, the PVPS participants have been conducting a variety of joint projects in the application of photovoltaic conversion of solar energy into electricity.

The mission of the IEA PVPS programme is: To enhance the international collaborative efforts which facilitate the role of photovoltaic solar energy as a cornerstone in the transition to sustainable energy systems.

The underlying assumption is that the market for PV systems is rapidly expanding to significant penetrations in grid-connected markets in an increasing number of countries, connected to both the distribution network and the central transmission network.

This strong market expansion requires the availability of and access to reliable information on the performance and sustainability of PV systems, technical and design guidelines, planning methods, financing, etc., to be shared with the various actors. In particular, the high penetration of PV into main grids requires the development of new grid and PV inverter management strategies, greater focus on solar forecasting and storage, as well as investigations of the economic and technological impact on the whole energy system. New PV business models need to be developed, as the decentralised character of photovoltaics shifts the responsibility for energy generation more into the hands of private owners, municipalities, cities and regions.

The overall programme is headed by an Executive Committee composed of representatives from each participating country and organization, while the management of individual research projects (Tasks) is the responsibility of Operating Agents. By late 2013, fourteen Tasks were established within the PVPS programme, of which six are currently operational.

The overall objective of Task 13 is to improve the reliability of photovoltaic systems and subsystems by collecting, analysing and disseminating information on their technical performance and failures, providing a basis for their assessment, and developing practical recommendations for sizing purposes.

The current members of the IEA PVPS Task 13 include:

Australia, Austria, Belgium, China, the European Photovoltaic Industry Association (EPIA), France, Germany, Israel, Italy, Japan, Malaysia, the Netherlands, Norway, Spain, Sweden, Switzerland, Turkey and the United States of America.

Performance characterization for thin-film PV modules requires special care because of the complex nature of the devices compared to first-generation PV devices. This report addresses the characterization of PV modules in solar simulators and in field conditions. We review the previous work on best practices for pre-conditioning and indoor measurements and propose a new method for stabilisation of modules without light exposure. Special considerations for bifacial PV modules are also discussed. After summarizing previous studies on characterization of field performance, we present a new, uniform analysis of international field data from many contributors. Finally, we present case studies related to the effects of spectrum on outdoor performance.

The editors of the document are Timothy J Silverman, National Renewable Energy Laboratory, Golden, CO, USA, and Ulrike Jahn, TÜV Rheinland Energie und Umwelt GmbH, Cologne, Germany (DEU).

The report expresses, as closely as possible, the international consensus of opinion of the Task 13 experts on the subject at hand. Further information on the activities and results of the Task can be found at: <http://www.iea-pvps.org>.

2 Executive Summary

Although thin-film photovoltaic (PV) modules have been in production for decades, the characterization of their performance, both outdoors and under artificial light, remains a topic of active research. This is because the field contains a diverse set of PV technologies, each of which has physical differences from conventional crystalline silicon PV. These differences range from different temperature coefficients to complex short-term or seasonal transients in performance. This report summarises the nature of these special behaviours and demonstrates best practices for handling them in the context of several case studies.

The first portion of the report deals with the performance of thin-film PV modules in solar simulators. Achieving repeatable performance measurements is challenging, even under artificial light. Stable, spectrally matched reference modules are generally unavailable, which can lead to errors in the effective illumination level. Some technologies have high capacitance, leading to problematic dependence of results on the duration of illumination and of the I-V curve sweep. Modules must be stabilised to avoid the influence of metastabilities on the results. This is normally done by light exposure or “light soaking” and the report proposes an approach for improving upon simple light soaking by applying bias.

The report then covers the issues surrounding the measurement and analysis of outdoor performance of thin-film PV modules. The widely varying spectral responses, temperature coefficients and metastable behaviours of different thin-film technologies lead to special challenges in outdoor performance analysis. This is illustrated by the presentation of a new method of collecting and analyzing performance data from many international partners. Specific issues of spectral performance analysis are then discussed, including measured-spectrum and modeled-spectrum methods.

The target audience of the report is scientists and engineers who participate in the collection, analysis and prediction of indoor and outdoor performance data. This group includes planners,

operators and manufacturers of PV power plants, participants in the standardization of methods for performance measurement and workers in academe or at national laboratories.

3 Simulator Performance

3.1 Previous work

3.1.1 Introduction

G Friesen, University of Applied Sciences of Southern Switzerland (SUPSI)

A Louwen and WGJHM van Sark, Utrecht University, Copernicus Institute of Sustainable Development, the Netherlands

Characterizing the performance of thin-film PV modules indoors is complicated by several physical differences between thin-film and conventional crystalline silicon PV technology. These differences can result in substantial scatter when the same module is measured in different ways or at different laboratories. Endeavors that rely on the repeatability of indoor performance measurements must be undertaken with these issues in mind.

The following contribution summarises a campaign of round-robin tests intended to characterise and reduce the uncertainty in performance measurements from multiple laboratories. This section is followed by a review of literature enumerating the various phenomena that contribute to the difficulty in achieving repeatable indoor performance measurements.

3.1.2 State of the art in indoor performance characterization of PV modules with solar simulators

This chapter summarises results of previous international studies, which can be considered to be representative of the state of the art of thin-film module characterization and its progress compared to the better-investigated characterization of crystalline silicon modules. Most of the work referenced here is from the European project IP PERFORMANCE (IP Contract 019718), which ended in 2010.

One of the major objectives of the PERFORMANCE project was to improve the accuracy and comparability of electrical power measurements of PV modules. Thus, standard test conditions (STC) were considered, as well as all test conditions defined within the IEC 61215 [1] and IEC 61646 [2] module qualification standard: STC (1000 W/m², 25°C, AM1.5); different module temperatures (800 W/m², 25-65°C, AM1.5), nominal operating cell temperature (800 W/m², NOCT, AM1.5) and low irradiance (200 W/m², 25°C, AM1.5).

New test equipment and procedures were developed within the project, to improve the accuracy and to cover an even broader range of test conditions (100-1200 W/m² and 15-75°C), as requested by the upcoming IEC 61853 Energy Rating standard part 1 [3] and 2 [4].

The comparability of measurements was mainly assessed by the means of different measurement intercomparison campaigns, so-called round-robin tests. All major European test laboratories with broad experience in indoor and outdoor testing and ISO17025

accreditation participated in the round-robin tests. Two round-robin tests focused on crystalline silicon modules and two on thin-film modules. The whole range of commercially available products was considered. The execution of an initial round-robin with a follow-up round-robin enabled the verification of the level of improvement achieved by the introduction of new test procedures and equipment, all aiming to better meet the technology-specific requirements. The round-robin results have been published at the major European conferences [5-7] and merged into a “Best practice guideline for industry” [8].

Crystalline silicon round-robin results

Very good results have been achieved for all crystalline silicon modules tested within the round-robin, with a comparability of P_{max} of $\pm 1-1.5\%$ (see Fig. 1). For the majority of the modules the spread was below $\pm 1\%$. Only for high-efficiency modules, where special measurement techniques are required to overcome capacitive effects [8], does the spread reach $\pm 1.5\%$. New measurement techniques have been developed more recently for high-capacitance modules [9,10], and further round-robins are underway to assess the accuracy of these new methods. The spread was significantly higher at test conditions different from STC as shown in Fig. 2 and 3, but always within the limits of the declared measurement uncertainties $U[k=2]$. All measurement uncertainties were calculated according to a common approach agreed to within the PERFORMANCE project and published by Müllejans et al. [11], which covers all relevant optical, electrical and measurement related factors. The increase of the spread up to $\pm 4\%$ for low irradiance levels can be mostly explained by the increase in non-uniformity of the solar simulators when introducing spectral neutral filters for the attenuation of irradiance, whereas the spread of up to $\pm 10\%$ for the temperature coefficient of P_{max} can be mostly explained by the differences in test procedures and equipment available in the different laboratories.

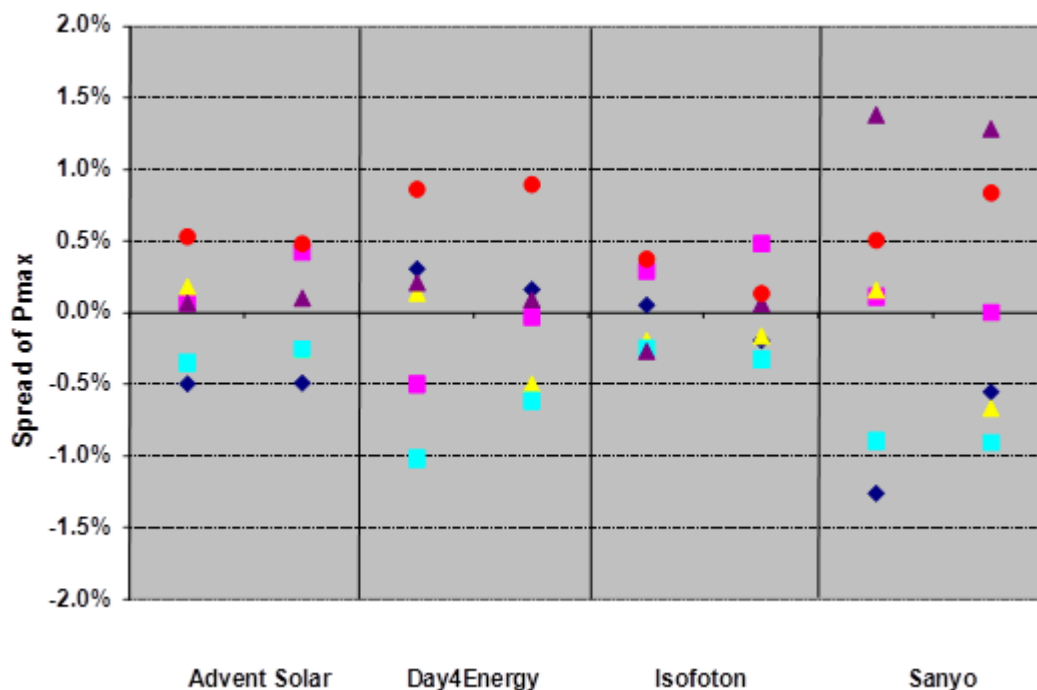


Fig. 1: Spread of P_{max} at STC (deviation from average of six test laboratories) as measured with different solar simulators and four different crystalline silicon module types

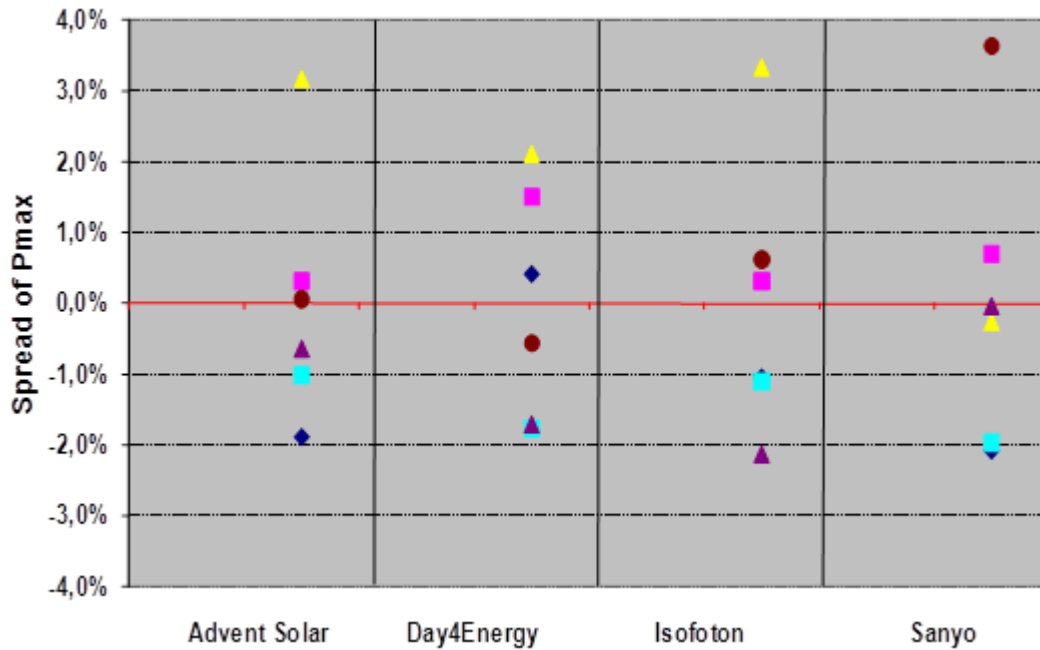


Fig. 2: Spread of P_{max} at 200 W/m² (deviation from average of six test laboratories) as measured with different solar simulators and four different crystalline silicon module types

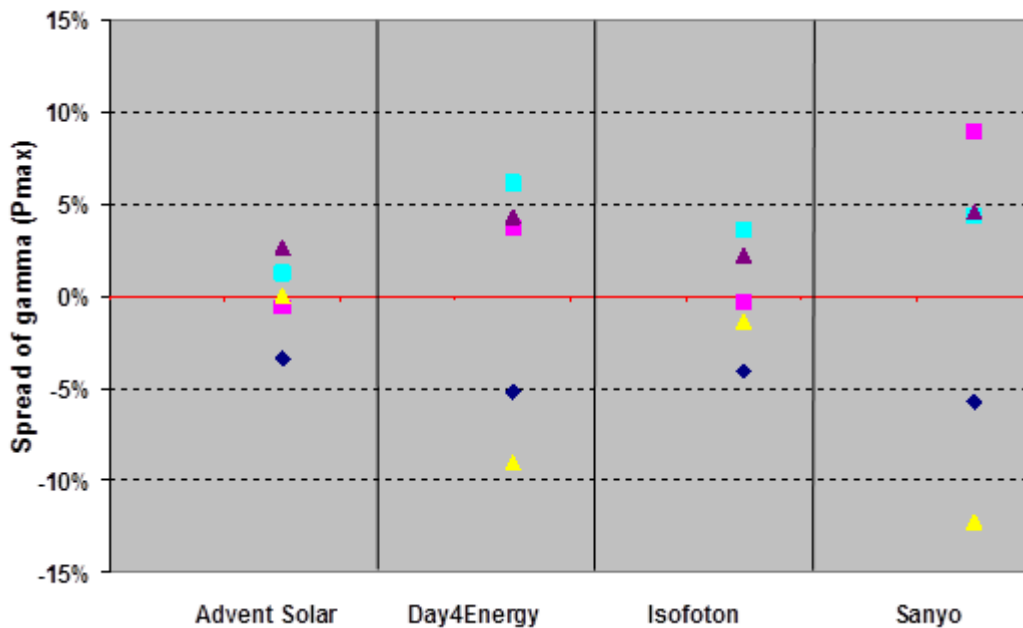


Fig. 3: Spread of P_{max} temperature coefficient measured at 800 W/m² (deviation from average of six test laboratories) as measured with different solar simulators and four different crystalline silicon module types.

Thin-film round-robin results

For thin-film modules the electrical characterization turned out to be much more difficult [6, 7] and the round-robin was therefore limited to the characterization under STC. Electrical instability of the material in combination with non-harmonised preconditioning techniques, spectral mismatch problems caused by the unavailability of perfectly spectral matched reference devices or spectrally tunable solar simulators, as well as the current limiting behaviour of sub cells within multi-junction modules, resulted in a poorer comparability of

power measurements of thin-film modules. Fig. 4 gives an overview of the results obtained with the final round-robin. Depending on the technology, a comparability of P_{max} within 3-6% was achieved for P_{max} at STC, with the best result for crystalline silicon on glass (CSG) where instability and spectral mismatch issues are less critical. A general improvement could be demonstrated within the project from the first to the second thin-film round-robin by harmonizing the stabilisation procedures. The following paragraphs highlight some technology-specific problems that could not be solved within the PERFORMANCE project and which will be treated in more detail throughout the whole report.

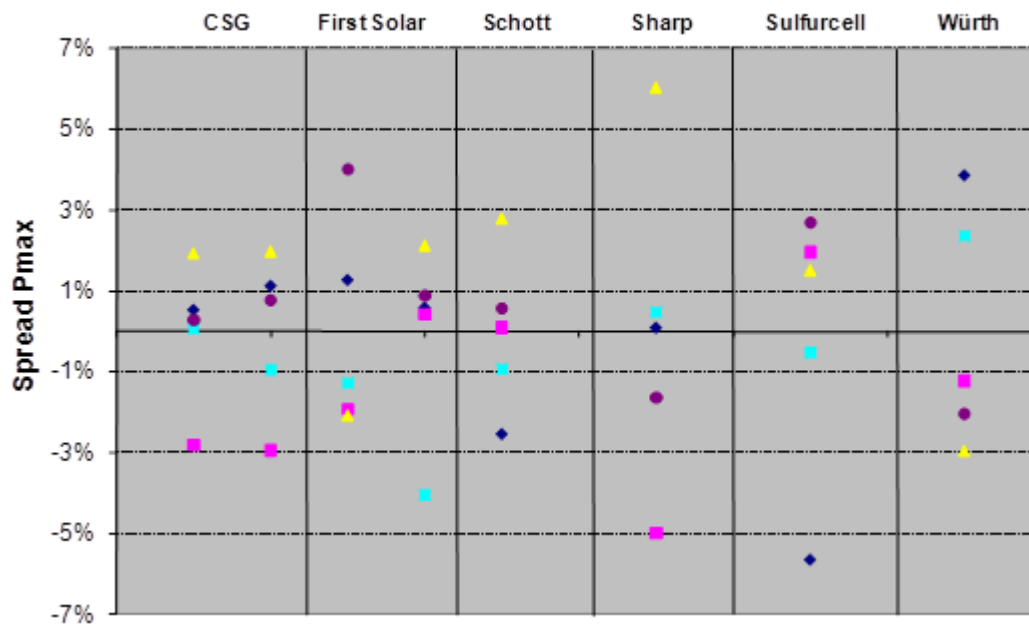


Fig. 4: Spread of P_{max} at STC (deviation from average of six test laboratories) as measured with different solar simulators and four different thin-film module technologies within the second round-robin

For amorphous silicon the standard approach according to IEC 61646 was applied to stabilise the module power, but with a stricter limit of $\pm 1\%$ for the second round-robin. It was observed that the stabilisation within $\pm 2\%$ did not fully stabilise the modules, and the stabilisation process continued during the execution of the round-robin, leading consequentially to a higher spread. Thermal annealing was avoided by monitoring the module temperature during the whole round-robin process and by not exposing the modules to temperatures above 50°C .

For copper indium (gallium) diselenide (CIS) and cadmium telluride (CdTe) a 1-hour outdoor exposure under load at irradiance above 800 W/m^2 and temperature below 55°C was agreed upon for pre-conditioning. A better comparability was achieved, but without being able to guarantee full stability. Moreover, no harmonised procedure was suggested on how to deal with the effects occurring during the timeframe from when the module is transported to the solar simulator and the module is cooled down to 25°C .

The spectral mismatch error has been identified as a major issue for the characterization of all thin-film technologies. An accurate measurement of spectral response and solar simulator spectrum are of primary importance for spectral mismatch corrections or the estimation of the

spectral mismatch error when no spectral correction is applied. At the time of the project, only one laboratory was able to measure the spectral response of complete modules and only of single-junction devices. These measurements together with some spectral response curves measured on the cell level have been distributed to all round-robin partners for the selection of the best reference device and/or to perform spectral mismatch corrections. The comparability between cell and module were very good, but the transferability of measurement results from cell to module level has still to be demonstrated for all technologies. The spectra of the solar simulators have all been measured with the same spectral radiometer, but without considering variations over time caused by lamp aging or other issues. Later studies showed that thin-film modules are particularly sensitive to spectral variations caused by the aging of the lamps or other issues [12]. Also, the equipment for the spectral characterization of solar simulators is under continuous investigation [13, 14]. New test equipment for the measurement of spectral response curves of single and multi-junction modules has been introduced in the meantime by most test laboratories [15,16,17], but too late to be included into the PERFORMANCE round-robin campaigns.

3.1.3 Specific issues in thin-film modules

The round-robin results have highlighted some unresolved issues, which will be the main focus of this report. Most of these issues are related to thin-film modules. A clear need for further improvements was identified in the field of pre-conditioning of CIS and CdTe, the testing of multi-junction devices, better spectral characterization of modules and solar simulators, and the understating of seasonal variations within thin-film modules.

In the following sections, we give a short overview of the major issues that can occur with thin-film technologies. Further information can be found in the “Best practice guideline for industry” [4] published within the PERFORMANCE project.

Metastability and stabilisation procedures

Because of the metastable nature of the semiconductor materials, achieving precise power measurements on thin-film PV modules often requires the application of a stabilisation procedure prior to each measurement. According to the various physical mechanisms behind the transient behaviours, many stabilisation techniques have been proposed. Some copper indium gallium diselenide (CIGS) and CdTe manufacturers have helped test laboratories to achieve higher power measurement accuracy by developing and sharing specific stabilisation procedures for their own products.

Amorphous silicon

Single-junction amorphous silicon modules are well known to exhibit significant performance degradation in the first few hundred hours of operation. This performance degradation leads to a decrease of efficiency of ~10-30% [18], while a typical value is reported to be 16% [19]. After several months of operation, degradations of even 30% to 40% were observed [19]. This degradation is the result of a material degradation effect known as the Staebler-Wronski Effect (SWE). With thermal annealing, this performance degradation can be partly recovered [19], [18]. The strength of the effect is reported to be related to the device structure; devices with thinner intrinsic layers exhibit less performance loss [18, 19], because of decreased recombination of photocarriers [18].

The degradation necessitates preconditioning or stabilisation [19, 20]. Outdoor measurements show rapid decrease in photocurrent in the first days of operation, and similar performance degradation after 6 weeks of operation [15]. In IEC 61646 it is stated that stabilisation can be assumed after 43 kWh/m² of irradiation is applied and power output changes less than +/-2%. Astawa et al [20] show that in order to perform accurate degradation measurements, loading of the modules should be performed under realistic operating conditions (operation at maximum power point). The practice of exposure to light, being indoor or outdoor, under open-circuit conditions, leads to an overestimation of V_{oc} degradation by 23% and an underestimation of I_{sc} degradation by 7.69% [20].

Cadmium telluride

The indoor characterization of CdTe modules is complicated by two factors: spectral mismatch (discussed in the next section) and short-time light soaking effects [21]. Light soaking leads to an initial performance improvement of ~4% [18], which necessitates preconditioning before performing indoor performance characterization. The effect can be reversed through dark storage [18].

Copper indium diselenide

CIS modules are known to exhibit “beneficial reversible metastability under light soaking”, which necessitates preconditioning before testing device performance indoors [18]. In [21] unconditioned CIS modules showed P_{max} measured indoors to be 94% of that measured outdoors. This light soaking effect can be reversed by annealing at 80°C in the dark [18]. Preconditioning times were found to be shorter when preconditioning was performed at higher temperatures [18].

Spectral considerations for indoor measurements

As we have seen in previous sections, the effect of spectral variations on thin-film PV performance can be quite pronounced. Especially for amorphous silicon (a-Si) and CdTe, this means indoor characterization of modules should consider the incident spectrum of the solar simulator, and correct for discrepancies between the simulator and solar irradiation at standard test conditions.

Fig. 5 shows an overview of the effect of spectral mismatch on indoor characterization of different PV parameters, for different thin-film technologies. Measurements for a-Si and CdTe need correction for spectral mismatch because of the large discrepancy between the spectral response of a-Si and CdTe on the one hand, and the c-Si reference cell on the other [21]. For CIS, which has a very similar spectral response compared to c-Si, this effect is very much smaller [21].

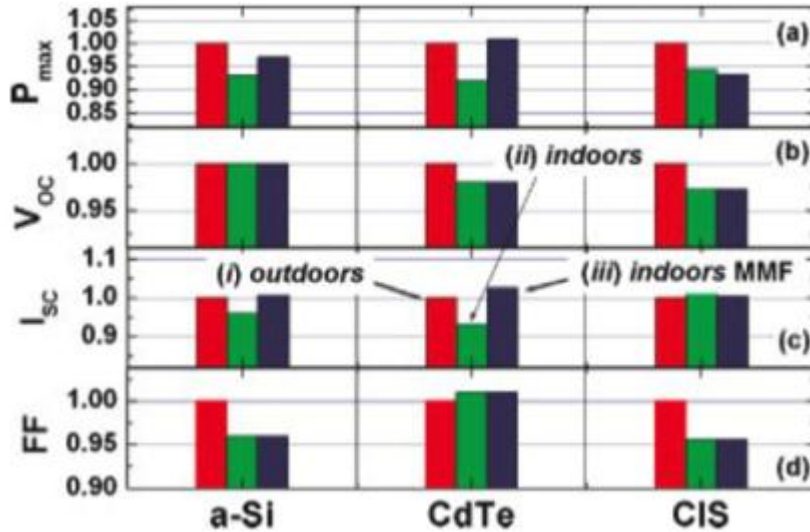


Fig. 5: Normalised PV parameters of single junction thin-film devices as measured (i) outdoors, (ii) indoors without spectral mismatch correction, and (iii) indoors with spectral mismatch correction. The variations are relative to the outdoor measurement [21].

Capacitive phenomena and I-V sweep time effects

Current-voltage characteristics are measured by sweeping voltage from slightly below zero to above V_{oc} , which takes a finite time. It has been found that I-V curves may differ as a function of sweep time. Of the thin-film technologies, only a-Si (single, double and hybrid a-Si/ μ c-Si) shows appreciable sweep time effects. For single-junction a-Si devices, sweep time effects occur up to 10 ms [21]. For double-junction and hybrid a-Si, similar results were obtained, so for these technologies, I-V measurements should be performed with sweep times >10 ms [21]. For CdTe and CIS, no sweep time effects were found. Fig. 6 shows the effect of sweep-time for the different thin-film technologies mentioned.

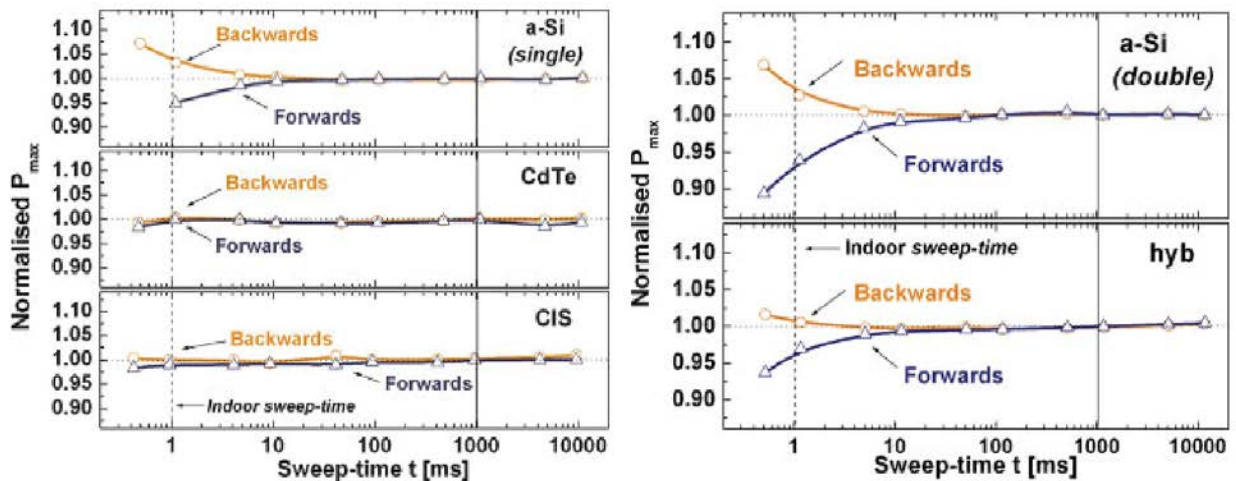


Fig. 6: Normalised power (P_{max}) of single-junction thin-film devices (left) and double-junction and hybrid a-Si (right) module, measured as a function of I-V sweep-time. The dashed line indicates a typical sweep-time used for the LAPSS solar simulator [21].

References for this section

- [1] IEC 61215 (2005): Crystalline silicon terrestrial photovoltaic (PV) modules – Design qualification and type approval.
- [2] IEC 61646 (2008): Thin-film terrestrial photovoltaic (PV) modules – Design qualification and type approval.
- [3] IEC 61853-1 edition 1.0. (2011): Photovoltaic (PV) Module Performance Testing and Energy Rating - Part 1: Irradiance and Temperature Performance Measurements and Power Rating.
- [4] IEC 61853-2 FDIS: Photovoltaic (PV) Module Performance Tasting and Energy Rating - Part 2: Spectral Response, Incidence Angle and Module Operating Temperature Measurements.
- [5] W. Herrmann, S. Mau, F. Fabero, T. Betts., N. van der Borg, K. Kiefer, G. Friesen, W. Zaaiman, Advanced intercomparison testing of PV Modules in European test laboratories, Proc. 22nd EU PVSEC, Milan, Italy, (2007), pp. 2506-2510.
- [6] W. Herrmann, S. Zamini, F. Fabero, T.R. Betts, N.J.C.M. van der Borg, K. Kiefer, G. Friesen, W. Zaaiman, Results of the European PERFORMANCE Project on Development of Measurement Techniques for Thin-Film PV Modules, Proc. 23rd EU PVSEC, Valencia, Spain, (2008), pp. 2719 – 2722.
- [7] W. Herrmann, S. Zamini, F. Fabero, T. Betts, N. van der Borg, K. Kiefer, G. Friesen, H. Müllejans, H.-D. Moring, M.A. Vázquez, D. Fraile Montoro, PV Module Output Power Characterization in Test Laboratories and in the PV Industry - Results of the European PERFORMANCE Project, Proc. 25th EU PVSEC / 5th World PVSEC, Valencia, Spain, (2010), pp. 3879 – 3883.
- [8] E. Dunlop, F. Fabero, G. Friesen, W. Herrmann, J. Hohl-Ebinger, H.-D. Moring, H. Müllejans, A. Virtuani, SUPSI W. Warta, W. Zaaiman, S. Zamini, Guideline for PV power measurement in industry, EUR 24359 EN, (2010).
- [9] A. Virtuani, P. Beljean, G. Rigamonti, G. Friesen, D. Chianese., Fast and accurate methods for the performance testing of highly efficient c-Si Photovoltaic modules using a 10 MS single-pulse solar simulator and customised voltage profiles, Meas. Sci. Technol. 23 (2012) 115604 pp. 1-8, doi:10.1088/0957-0233/23/11/115604
- [10] C. Monokroussos, D. Etienne, K. Morita, C. Dreier, U. Therhaag, W. Herrmann, Accurate Power Measurements of High Capacitance PV Modules with Short Pulse Simulators in a Single Flash, Proc. 27th EU PVSEC, Frankfurt, Germany, (2012), pp. 3687 – 3692.
- [11] H. Müllejans, W. Zaaiman, R. Galleano; Analysis and mitigation of measurement uncertainties in the traceability chain for the calibration of photovoltaic devices; Measurement Science and Technology 20, (2009), 075101 pp. 1-12
- [12] W. Herrmann, L. Rimmelspacher, Uncertainty of Solar Simulator Spectral Irradiance Data and Problems with Spectral Match Classification, Proc. 27th EU PVSEC, (2012), pp. 3015 – 3021.
- [13] P. Sperfeld, D. Dzafic, F. Plag, F. Haas, C. Kröber, H. Albert, S. Nevas, S. Pape, Usability of Compact Array Spectroradiometers for the Traceable Classification of Pulsed Solar Simulators, Proc. 27th EU PVSEC, Frankfurt, Germany, (2012), pp. 3060 – 3065.
- [14] D. Polverini, R. Galleano; The use of fast spectroradiometers for pulsed solar simulator spectra measurements, Proc. 37th IEEE PVSC, Seattle, WA, USA, (2011) pp. 003596-003600.
- [15] M. Pravettoni, M. Nicola, G. Friesen, A Filtered Pulsed Solar Simulator for Spectral Response Measurements of Multi-Junction Modules of Commercial Size, Proc. 27th EU PVSEC, Frankfurt, Germany, (2012), pp. 3209 – 3213.
- [16] F.P. Baumgartner, D. Schär, S. Achtnich, Spectral Response Measurement of Tandem Modules, Proc. 27th EU PVSEC, Frankfurt, Germany, (2012), pp. 3022 – 3026.
- [17] Y. Tsuno, Y. Hishikawa and K. Kurosawa, A Method for Spectralour Response Measurements of Various PV Modules, Proc. 23rd EU PVSEC, Valencia, Spain, (2008), pp. 2723 – 2727.
- [18] M. Gostein and L. Dunn, Light soaking effects on photovoltaic modules: Overview and literature review, Proc. 37th IEEE PVSC, Seattle, WA, USA, (2011), pp. 3126–3131.

[19] M. Muñoz-García and O. Marin, Characterization of thin-film PV modules under standard test conditions: Results of indoor and outdoor measurements and the effects of sunlight exposure, *Solar Energy*, vol. 86, no. 10, (2012), pp. 3049–3056.

[20] K. Astawa, T. R. Betts, and R. Gottschalg, Effect of loading on long term performance of single junction amorphous silicon modules, *Solar Energy Materials and Solar Cells*, vol. 95, (2011), pp. 119–122.

[21] A. Virtuani, Comparison of indoor and outdoor performance measurements of recent commercially available solar modules, *Progress in Photovoltaics: Research and Applications* 19.1 (2011), pp. 11–20.

3.2 Stabilisation issues particular to thin-film PV modules

3.2.1 Introduction

Determining the STC power rating of a thin-film PV module is important for predicting outdoor performance and for quantifying degradation caused by outdoor exposure or by accelerated testing. This otherwise simple measurement is frustrated by the fact that most polycrystalline thin-film PV modules exhibit some form of transient change in performance on time scales of a few days or less. Modules must therefore be stabilised before their STC power rating can be determined. The development of stabilisation methods that apply to all thin-film PV technologies continues to be an active area of research because each technology, and in some cases each specimen of a particular technology, behaves differently.

The following contribution is a report of new data showing the temperature dependence of the light-soaking effect on a large population of full-size modules. This information helps to illustrate the variety of transient responses that is possible in polycrystalline thin-film PV modules. The section is followed by a recommended approach for further development of procedures that do not rely solely on light exposure to achieve stabilisation.

3.2.2 Recent results in thin-film stabilisation

Markus Schweiger, TÜV Rheinland

Introduction

The physical processes of metastable behaviour of CIGS and CdTe modules are not understood yet [1]. IEC 61646 [2] contains the only standardised stabilisation procedure for thin-film PV-modules. This procedure does not take into account the technology-specific characteristics of the different thin-film technologies.

The metastable behaviour of 22 specimens has been investigated. Three CIGS module types from two different manufacturers and two CdTe module types from two different manufacturers have been measured indoors. The change of the main module parameters I_{sc} , V_{oc} and P_{max} was monitored online while light-soaking and by regular re-measurements in a pulsed solar simulator. The P_{max} was recorded every 30 seconds and the entire I-V curve was measured at 120-second intervals. The influence of the module temperature during the stabilisation was investigated for 25°C, 50°C and 85°C. The irradiance during the stabilisation process was 1000 W/m². The effect of small fluctuations of the module temperature and the irradiance have been corrected according to IEC 60891 [3] procedure 2. After the stabilisation program the modules were stored in the dark at 25°C with periodic I-V measurement to monitor their de-stabilisation.

Stabilisation of CIGS specimens

CIGS modules stabilised at low temperatures (25°C, 50°C) showed a rise of the nominal power, compared to the initial value, of up to 8%. The changes occurred because of a rising fill factor and a rising open circuit voltage, as shown in Fig. 7. The short circuit current remained almost stable. Aging effects could be detected for some modules during stabilisation at higher module temperatures (85°C), as shown in Fig. 8. The nominal power dropped down to -9% for some module types. The irradiation of one 43 kWh/m² cycle according to IEC 61646 appeared to be sufficient.

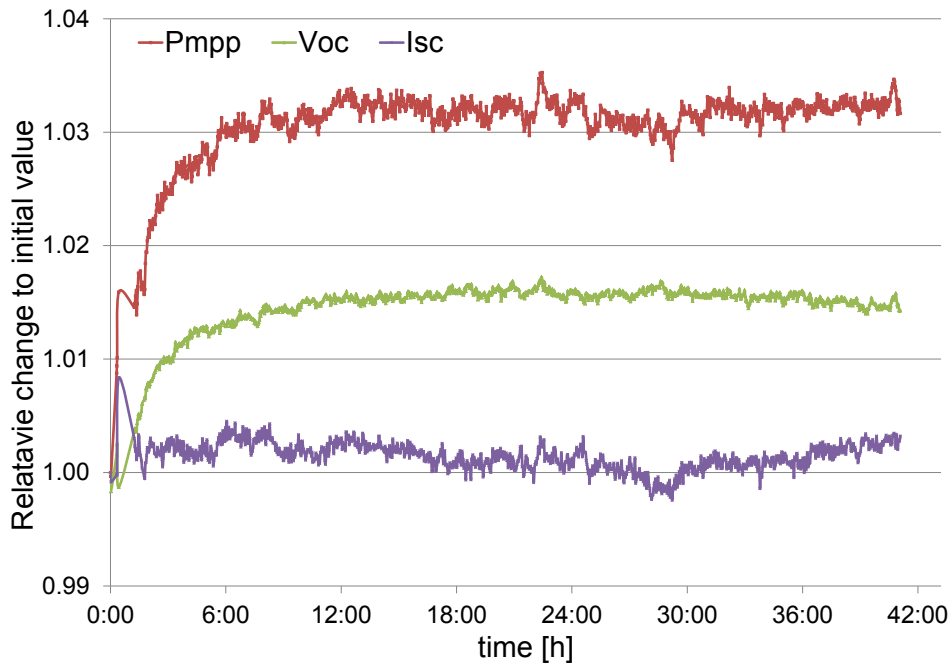


Fig. 7: Electrical stabilisation of a CIGS specimen during light-soaking at 1000 W/m² and a module temperature of 58.4°C

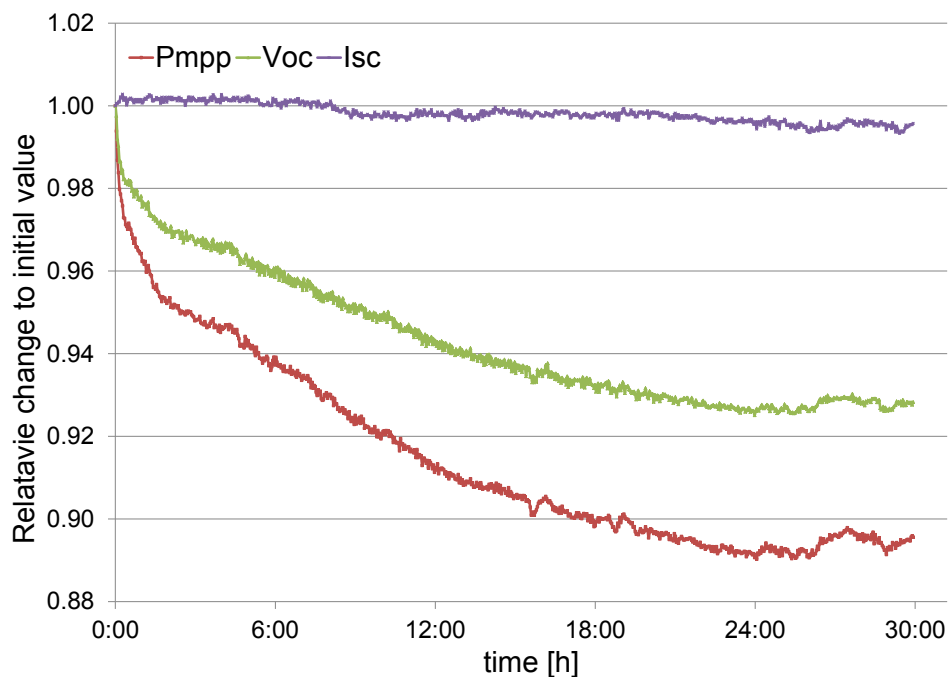


Fig. 8: Irreversible degradation of a CIGS specimen caused by light-soaking at 83.7°C module temperature, online-monitored module parameters at 1000 W/m²

Stabilisation of CdTe specimens

Most CdTe modules showed a rise of the nominal power compared to the initial value of up to 10%. The changes mostly occurred because of a rising fill factor, as shown in Fig. 9. The short-circuit current remains almost stable. In contrast to CIGS, the CdTe specimens showed a strong dependency of the stabilisation result on the module temperature during the stabilisation. The higher the module temperature was, the higher the resulting value of the nominal power. Low temperatures (25°C) led to small positive or even negative changes of nominal power, as shown in Fig. 10. A superposition of light-induced degradation and thermal activation can be assumed. Tests with high module temperatures and without exposure to light also showed a rise in the nominal power. The irradiation of one 43 kWh/m² cycle according to IEC 61646 also seems to be sufficient for CdTe.

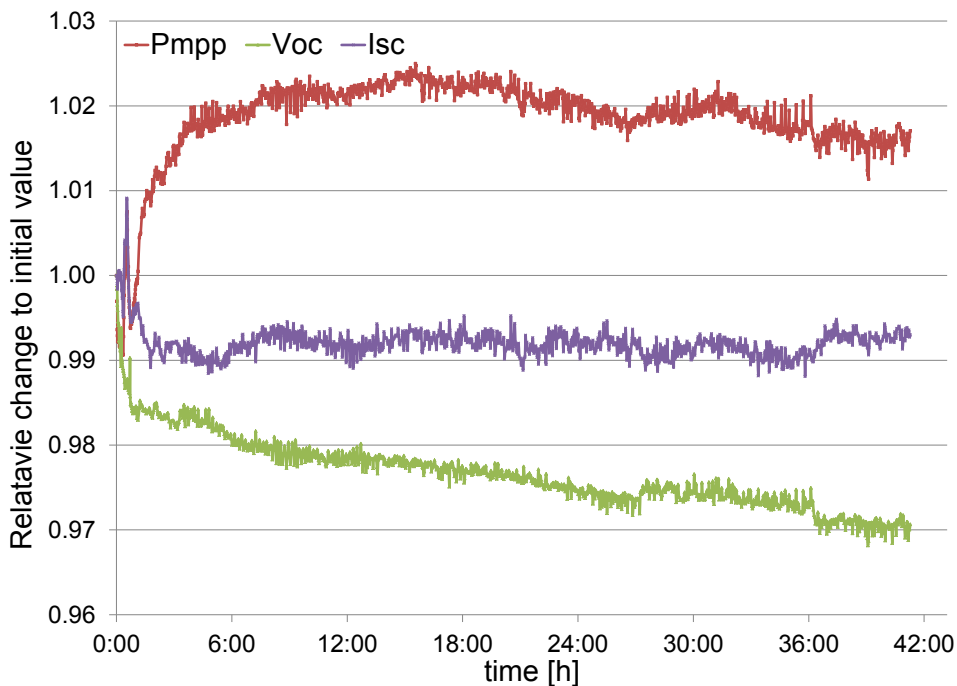


Fig. 9: Electrical stabilisation of a CdTe specimen during light-soaking at 1000 W/m² at a module temperature of 79.4°C

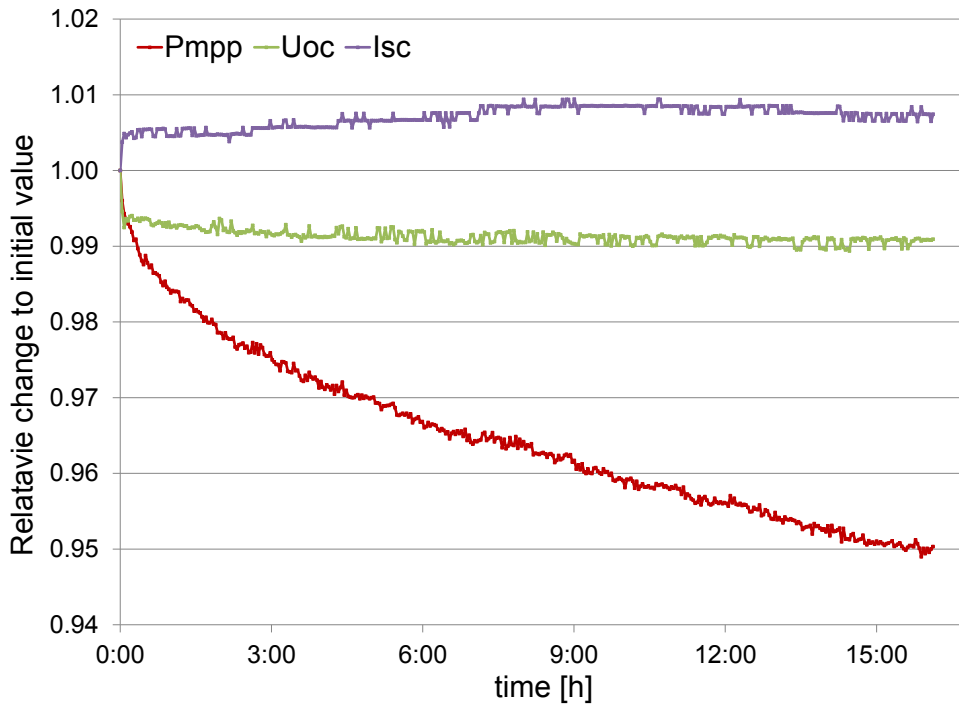


Fig. 10: Stabilisation of a CdTe specimen during light-soaking at 26.8°C module temperature and 1000 W/m²

Relaxation during storage in the dark

The reversal of stabilisation was investigated by storing the specimens in the dark at 25°C for several months and regularly performing re-measurements using the pulsed solar simulator. For both technologies (CIGS and CdTe), the results show long relaxation times of several weeks (Fig. 11 and 12). Some manufacturers state the destabilisation of their CIGS modules occurs within seconds. For these fast transient effects, another measurement approach must be chosen as described above.

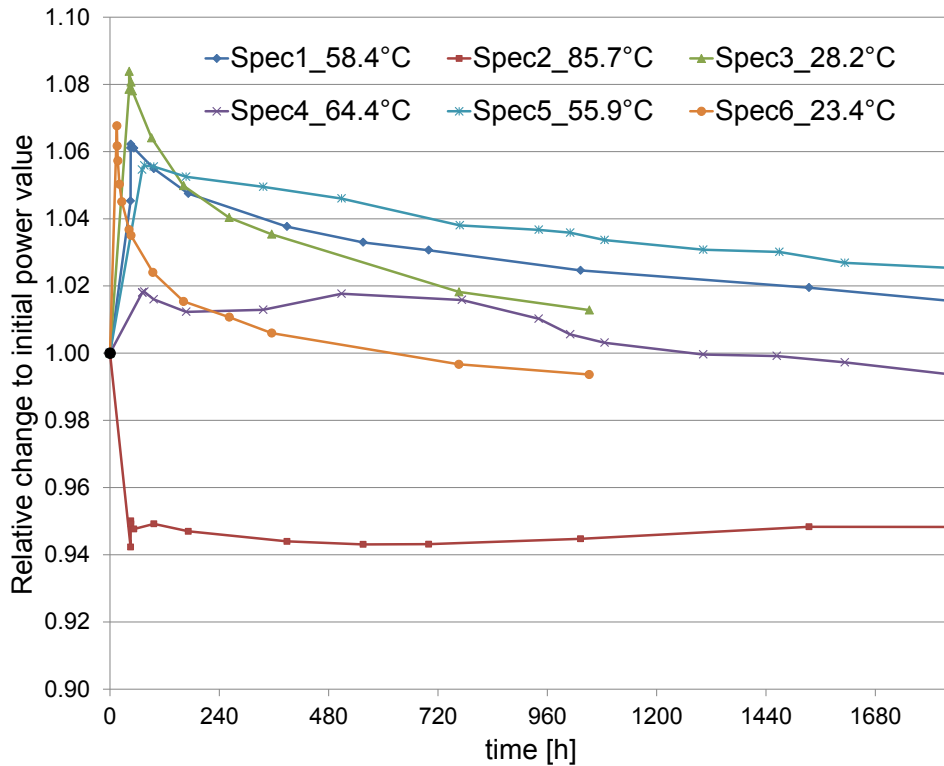


Fig. 11: Relative change of the nominal power of CIGS specimens during dark storage at various temperatures

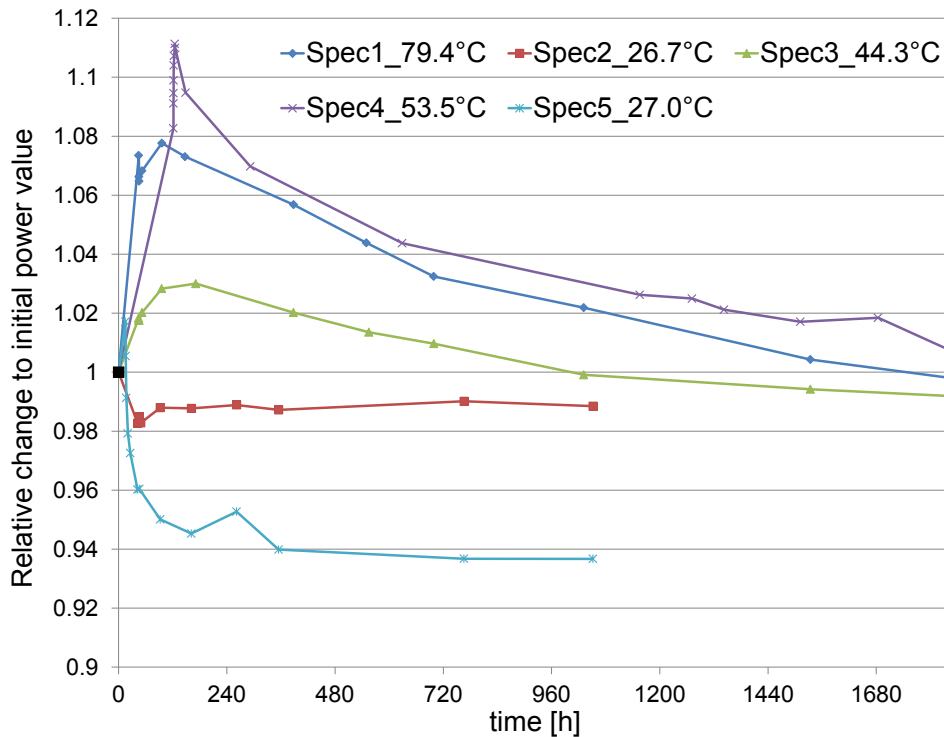


Fig. 12: Relative change of the nominal power of CdTe specimens during dark storage at various temperatures

References for this section

- [1] T. Eisenbarth: Identifikation von Defekten und Metastabilitäten in Cu(In,Ga)Se₂-Dünnschichtsolarzellen, (2010), Doctoral dissertation, Freie Universität Berlin.
- [2] IEC 61646: Thin-film terrestrial photovoltaic (PV) modules – Design qualification and type approval, (2008-05).
- [3] IEC 60891: Photovoltaic devices – Procedures for temperature and irradiance corrections to measured I-V characteristics, (2009-12).

3.2.3 Improving upon thin-film PV stabilisation methods

Timothy J Silverman, National Renewable Energy Laboratory, United States
Sabrina Novalin, Austrian Institute of Technology

Introduction

This chapter establishes the need to stabilise thin-film PV modules before measurement and describes the shortcomings of the light-soaking method of stabilisation. Improvements of the method, based on the use of bias in addition to or in place of illumination, are proposed. The specific tests needed to develop these improvements are proposed and results from pilot tests on CIGS modules are presented.

Background

The dominant thin-film photovoltaic materials, namely CdTe, CIGS and a-Si, all exhibit transient changes in performance upon exposure to light [1-3]. These effects influence current-voltage parameters and can result in either artificially high or low performance. The metastable effects vary in magnitude and can be observed in cells and modules alike. In some cases the effects might be close to measurement accuracy or even non-existent. However, in other cases, the performance of the cell or module can vary more than 10% above an initially measured value. Both the open-circuit voltage (V_{oc}) and the fill factor (FF) can be affected by these transients, and generally speaking, a partial or full relaxation to an originally measured value can be obtained by dark storage at 25°-80° C within times widely varying among the technologies (from hours to weeks). Fig. 13 and 14 show a time evolution of current-voltage characteristics upon light exposure which was observed for a CdTe module. After dark storage, the curves typically relax to the initial condition.

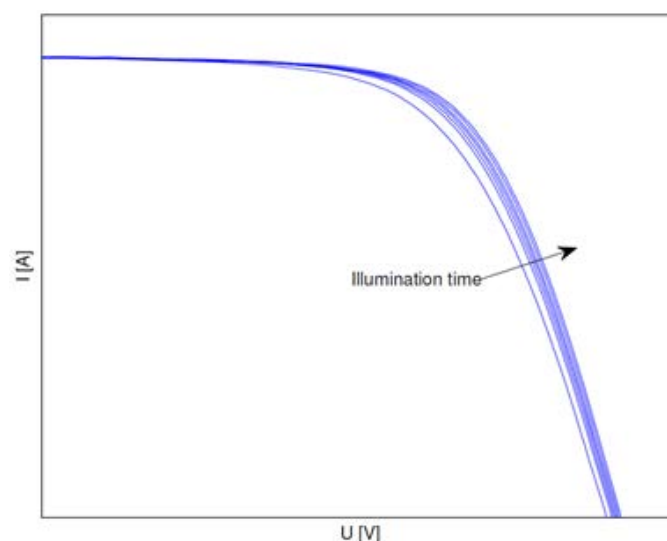


Fig. 13: Metastable evolution of the current-voltage characteristic measured for a CdTe module upon light exposure

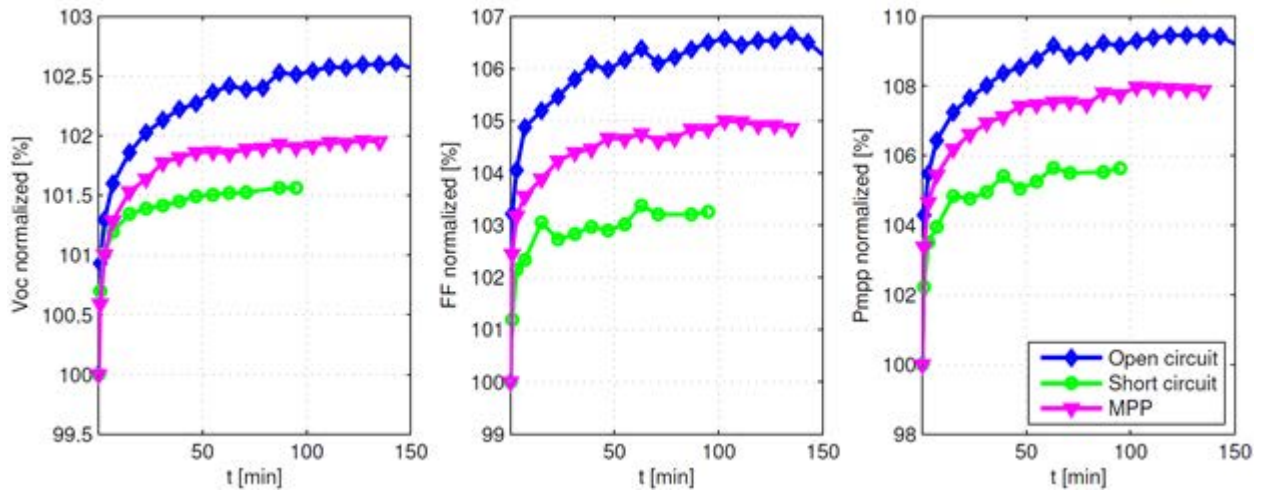


Fig. 14: Open circuit voltage (V_{oc}), fill factor (FF) and maximum power (P_{max}) of a commercial CdTe module depending on light exposure time and electrical bias

Nevertheless, the metastable behaviour does interfere with performance measurements when such measurements are made shortly after manufacture or after extended periods in darkness, such as during shipment or accelerated testing. It is important for performance measurements to reflect post-transient performance because this is a PV module's normal operating state. There is, thus, a need to "stabilise" modules, bringing them to their normal outdoor state, when measuring their performance after manufacture or darkness.

Modules can exhibit a great variety of transient behaviours with diverse physical origins operating at a wide range of time constants [1]. We focus on the ones most troublesome for performance measurements: reversible transients with time constants on the order of minutes or hours. Long-term transients are too easily confounded with degradation, and irreversible transients are not of concern for repeated measurements of the same module.

The most direct method of stabilising thin-film PV modules is to expose them to light until their performance no longer changes. A specific version of this approach is promulgated in the "light-soaking" process in International Standard IEC 61646. The process entails repeated exposure of a module to light in increments of $\geq 43 \text{ kWh/m}^2$ until the module's power value no longer changes by more than 2% between measurements. The standard allows the 43 kWh/m^2 exposure increments to occur over any length of time, containing any number of dark periods. It does not specify how soon after exposure a performance measurement must be made.

In CIGS and CdTe cells, bias can cause transient performance changes that are similar to those caused by illumination. The effect was observed in CIS in the 1980s [6], and in the 1990s it was shown that placing CIS and CdTe cells in forward bias can reduce the transient in V_{oc} that occurs upon illumination [7]. The process was tested on full-sized CIGS and CdTe modules in 2010. Although similar changes were observed between biased and light-exposed modules, it was not possible to establish the equivalence of bias to light exposure [8].

Potential for improvements

The IEC 61646 light-soaking process was designed for amorphous silicon, which shows a substantial degradation in response to light exposure, but a very slow recovery at room

temperature. The procedure was not designed for metastabilities that may relax quickly at room temperature. For example, CIGS modules can return to their dark state within several hours [9], suggesting that nighttime periods occurring during an exposure can cause some of the light-soaking effect to be lost. Bringing modules to indoor measurement equipment from outdoors can introduce a substantial delay that is usually not measured or controlled. This exposure-measurement delay has been found to affect the measurement by allowing some of the light-soaking effect to be lost [10]. This effect taints comparisons between modules in the same batch and between different measurements of the same module. Whereas the IEC 61646 process works well for amorphous silicon, a different procedure should be developed for CIGS and CdTe modules that show faster relaxation after light exposure.

For CIGS and CdTe modules, there is evidence that the equivalence of light and forward-bias can be used to improve the stabilisation process. The main advantage offered by bias stabilisation is that of improved control. Bias stabilisation is not subject to change due to weather or day length. The exposure-measurement delay can be easily controlled and made very short. There might also be cost and speed advantages: an outdoor light-soaking setup or a continuous solar simulator might be replaced with an inexpensive DC power supply that could be operated continuously, eliminating lost time because of poor weather. Bias conditions might be identified that allow stabilisation to proceed much more rapidly than with light-soaking.

Proposal for development of new stabilisation methods

The objectives of developing new stabilisation methods are to make the stabilisation process better controlled, less expensive and faster than the existing light-soaking method. A new method must also produce equivalent or better results for a particular technology or for a specific module type. There is sufficient evidence to proceed with the investigation of two approaches for improving the light-soaking method with bias stabilisation: elimination of the dependence of performance results on the exposure-measurement delay and elimination of light exposure from the stabilisation process entirely.

In this section, we describe experiments undertaken on CIGS modules to aid the development of improved stabilisation methods. Until sufficient data are available to develop a standard test method, these experiments can be used to establish the efficacy of a proposed method on a specific module type.

Stabilisation during the exposure-measurement delay

We propose to determine whether placing a PV module in forward-bias during the delay between light exposure and characterization eliminates the sensitivity of the performance measurement to the length of the delay. To be successful, this approach must be equivalent to ordinary light soaking followed by immediate I-V curve measurement.

The test makes use of a set of matching modules. All modules are exposed to light outdoors or in a solar simulator until their performance no longer changes with time. Immediately upon removal from the light source, an I-V curve is collected in a flash solar simulator. With the exception of one control module, the modules are then immediately placed in forward-bias. A different constant-current bias condition may be used on each non-control module. Constant current is used so that moderate changes in temperature do not cause large changes in the

bias condition. I-V curves are collected at increasing time intervals until the exposure-measurement delay is several days.

The performance of the control module, which is stored in darkness between post-exposure measurements, is expected to gradually change throughout the experiment. If it does not, the module type under test does not require special treatment during the exposure-measurement delay.

One or more of the modules placed in forward-bias during the delay are expected to show no change in performance. Some modules may be damaged by the application of excessive current; this test may be able to distinguish the threshold below which there is no risk of damage. We suggest use of the lowest-current condition that maintains the module in its stabilised state during the delay. Preliminary results are shown in a later section from a pilot experiment on five types of CIGS modules.

Stabilisation without light exposure

Another proposed test is to determine the efficacy of forward-bias stabilisation with no light exposure at all. The objective is to establish a process that is better controlled, less expensive and faster than the light-soaking process. The test can also be used to determine the conditions under which forward bias is equivalent to light exposure.

The test makes use of a set of matching modules that have been stored in darkness for several weeks. An I-V curve is collected from each module at STC. With the exception of one control module, the modules are then placed in forward-bias at several different constant-current bias conditions. The voltage and temperature of the biased modules are continuously monitored. I-V curves are collected at increasing time intervals and the test proceeds when consecutive I-V curves are sensibly identical. All of the modules are then exposed to light and their P_{max} or V_{oc} continuously monitored.

The performance of the control module is expected not to change during the indoor portion of the test, then to exhibit its usual transient behaviour on exposure to light. If its performance does not change outdoors, no stabilisation is needed for this module type. If its performance changes during the indoor portion of the test, it may not have been in the dark state at the start of the test.

One or more of the remaining modules are expected to change in performance during the indoor portion of the test, then show no further change when deployed. The indoor performance measurements will reveal when the modules became fully stabilised. The temperature-corrected voltage measurements collected during bias can be used to establish a simple stopping criterion for achieving stability. If various indoor bias conditions are tested, the lowest-current condition that eliminates the transient upon light exposure can be identified. Preliminary results from this method are shown in a later section.

CIGS pilot tests and results

We performed pilot tests on CIGS modules based on both of the preceding proposals. The results show that further investigation of these methods is warranted.

Stabilisation during the exposure-measurement delay

To test exposure-measurement stabilisation, we used pairs of CIGS modules of five types [10]. Each type was tested at a different time. After extended storage in darkness, both modules were exposed outdoors for several days. The modules were then brought indoors and within 10 minutes, an initial I-V curve was measured at STC. One module was then immediately placed in forward-bias at I_{mp} (forward-biased dark storage) and the other was left at open-circuit (unbiased dark storage). I-V curves were collected from both modules at increasing time intervals up to 96 h.

With most module types, performance declined as expected during unbiased dark storage, as shown in Fig. 15. With the exception of CIGS D, the unbiased modules declined in P_{max} by $\geq 1\%$ within 1 hour and continued declining for the entire length of the experiment.

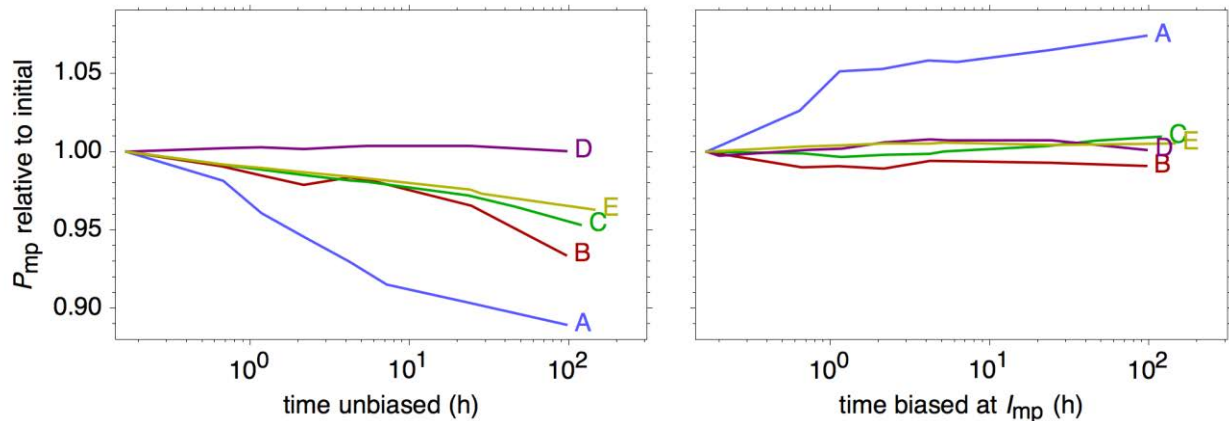


Fig. 15: Pairs of modules were repeatedly characterised after stabilisation by light-soaking. Between measurements, modules were stored in the dark unbiased (left) and biased at I_{mp} (right).

The forward-biased modules showed much smaller performance changes. With the exception of CIGS A, the forward-biased modules produced the same P_{max} , within 1% of the first measurement made indoors. CIGS A is thought to have shown anomalous behaviour either because its fast transient caused a decline in P_{max} during the ≤ 600 s exposure-measurement delay or because I_{mp} forward-bias caused an artificial enhancement in performance during the test.

The pilot data show that in many cases, placing a module in forward-bias at I_{mp} immediately upon removal from light exposure can eliminate the sensitivity of indoor performance measurements to the length of the delay between exposure and measurement. The exceptions are a module that showed no transient behaviour at all and one with such fast behaviour that the test was not conclusive. These results are sufficiently promising to continue testing this method with different module types, including CdTe modules, and with various bias conditions. These steps will enable the design of the ideal method for making measurements on modules with transient behaviour.

Stabilisation without light exposure

To determine the feasibility of bringing a module to its light-soaked performance level using bias alone, we used a pair of matching CIGS modules. Both modules were stored in darkness for several weeks. The test module was then placed in forward-bias at $I(V_{mp})$ and the control

module was left at open-circuit for several days. Both modules were then simultaneously deployed outdoors in sunny conditions, biased at the maximum power point.

The maximum power was monitored during outdoor exposure for several days. The results are plotted in Fig. 16. For the module type under test, stabilisation was achieved after <2 kWh/m² of exposure. The control module's P_{max} increased by 15% in the first day of exposure; the test module's P_{max} decreased by 3%. The bias stabilisation appears to have given the test module an artificial performance increase of 3%.

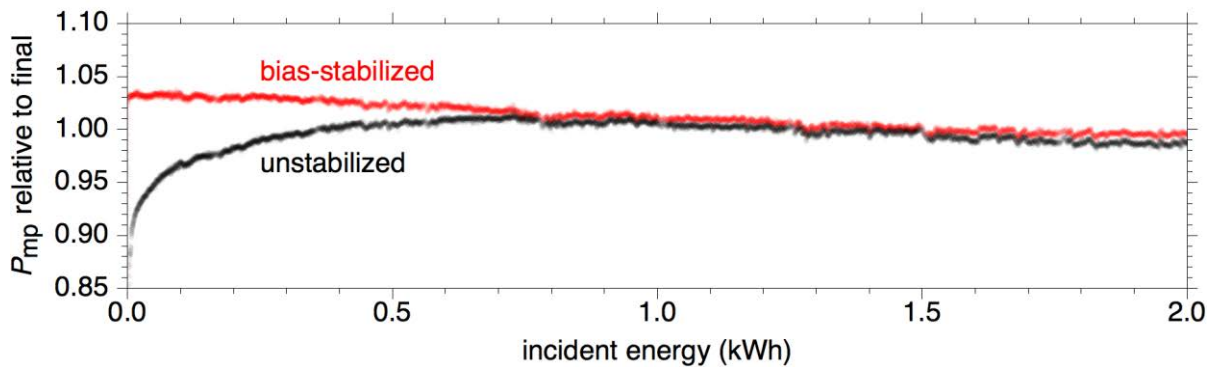


Fig. 16: Two modules were continuously measured upon outdoor exposure after unbiased dark storage (black points) and biased at $I(V_{mp})$ (red points). P_{max} is shown normalised to the final power and corrected for module back temperature and irradiance. [11].

The pilot data show that bias stabilisation with no light exposure at all is sufficiently promising to continue investigating the method. Further analysis can reveal what combinations of bias condition and duration can achieve stabilisation without producing an artificial performance increase. It can also be determined whether the test module's entire I-V curve, not just its P_{max} value, is brought to the same state as if it were stabilised with the light-soaking process. Tests on multiple module types can show under what conditions the method is effective and can aid in developing a stabilisation process that works for every module type or a set of stabilisation processes for individual application to different module types.

Conclusion

Pre-measurement stabilisation of thin-film PV modules has shortcomings that may be addressed by techniques involving the use of forward bias in addition to or in place of light exposure. We have suggested tests and provided promising pilot data to aid in the development of improved stabilisation methods. Stakeholders in thin-film PV characterization are encouraged to participate in this development so that an improved standard method can be established.

References for this section

- [1] M. Gostein, M. and L. Dunn, Light soaking effects on photovoltaic modules: Overview and literature review, Proc. 37th IEEE PVSC, Seattle, WA, USA, (2011), pp. 003126-003131.
- [2] S. Siebentritt, M. Igalson, C. Persson, S. Lany, The electronic structure of chalcopyrites - bands, point defects and grain boundaries, Prog. Photovolt: Res. Appl. 18 (2010), pp. 390–410.
- [3] J. A. del Cueto and B. von Roedern, Long-term transient and metastable effects in cadmium telluride photovoltaic modules, Prog. Photovolt: Res. Appl. 14 (2006), pp. 615-628.
- [4] A. Mittal, Master Thesis, Short Term Metastable Effects in the Amorphous Silicon Solar Modules, University of Oldenburg, Germany, (2012).
- [5] N. Taylor (ed.), Guidelines for PV Power Measurement in Industry, JRC Scientific and Technical Report EUR 24359 EN, doi:10.2788/90247, (2010).

- [6] M.N. Ruberto, and A. Rothwarf, "Time-dependent open-circuit voltage in CuInSe₂/CdS solar cells: Theory and experiment," J. Appl. Phys. 61 (9), (1987), pp. 4662-4669.
- [7] R.A. Sasala, and J.R. Sites, "Time dependent voltage in CuInSe₂ and CdTe solar cells," Proc. 23rd PVSC Louisville, KY, USA, (1993), pp. 543-548.
- [8] J.A. del Cueto, C.A. Deline, S.R. Rummel and A. Anderberg, "Progress toward a stabilisation and preconditioning protocol for polycrystalline thin-film photovoltaic modules," Proc. 35th PVSC, Honolulu, HI, USA (2010), pp. 002423-002428.
- [9] L. Dunn. and M. Gostein, "Light soaking measurements of commercially available CIGS PV modules," Proc. 38th IEEE PVSC, Austin, TX, USA, (2012), pp. 001260-001265.
- [10] C.A. Deline, A. Stokes, T.J. Silverman, S. Rummel, D. Jordan and S. Kurtz, "Electrical bias as an alternate method for reproducible measurement of CIGS photovoltaic modules," Proc. SPIE 8472, San Diego, California, USA, (2012), pp. 84720G-84720G.
- [11] B. Marion, "Comparison of predictive models for photovoltaic module performance." Proc. 33rd IEEE PVSC, San Diego, CA, USA, (2008), pp. 1-6.

3.3 Performance characterization of thin-film multi-junction PV cells and modules

Mauro Pravettoni, University of Applied Sciences of Southern Switzerland (SUPSI)
Marco Apolloni, TEL Solar, Switzerland

3.3.1 Introduction

The aim of this section is to examine current-voltage characterization of thin-film multi-junction cells and modules. In the absence of an international standard, which is under discussion at the time of this writing, the authors and contributors have tried to put together their know-how and the available national standards to draft a review of the basic principles. Literature works that have treated all challenging aspects to date are examined, including very recent ones. First, multi-junction photovoltaic devices are briefly introduced, including two challenging aspects: current-limitation and spectral mismatch. Then the specific problems that may be present in current-voltage characterization are addressed: choice of reference devices; requirements for solar simulators; the challenges in outdoor characterization and in spectral responsivity; and finally, the procedure for spectral mismatch correction according to the laboratory practice, with the definitions of the matching factor Z_i and of the current balance Bal_{ij} and their effect on the electrical parameters.

3.3.2 Theory and definitions

Multi-junction cells and modules

In a *multi-junction cell*, two or more PV junctions with decreasing bandgaps are stacked in optical and electrical series on top of each other. The junction with the widest bandgap faces the incoming irradiance and the one with the smallest bandgap is located at the bottom of the series, so that lower energy photons are able to pass through the top junctions and be absorbed by the bottom one. As a result, the total current is reduced, but the thermal energy loss of the high-energy photons is also reduced and the voltage is increased, with an overall positive effect on cell efficiency (see Fig. 17, where single- and multi-junction PV devices are compared to conventional batteries). A comprehensive work on multi-junction devices within third generation PV is included in the book by M. A. Green [1]; further information on thin-film multi-junction devices may also be found in Ref. [2].

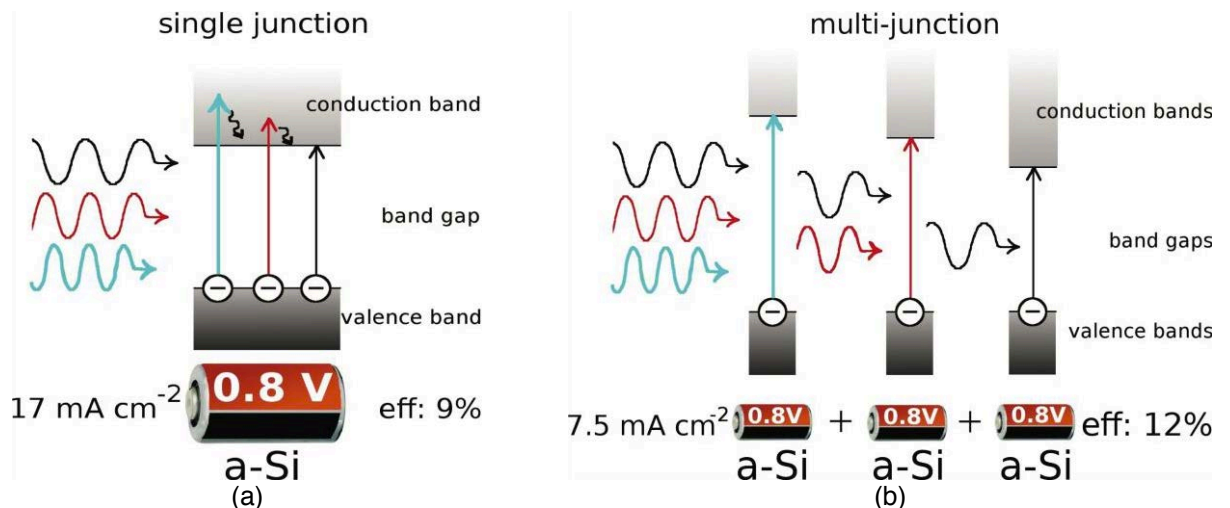


Fig. 17: Single and multi-junction PV devices compared to conventional voltage generators [3].

A well-known configuration of a multi-junction cell is the two-terminal *monolithic*: the junctions are grown on the top of each other and the electrical interconnection is provided by appropriate *tunnel-junctions* between each pair of sub-cells. The device is therefore *two-terminal* and electrical connection is possible to the total series of sub-cells. This technique is used to build multi-junction cells from the III-V group (InGaP/GaAs, InGaP/GaAs/Ge and so on), which because of their high manufacturing cost are usually only considered for aerospace applications and in concentrator systems.

Multi-junction thin-film cells based on amorphous silicon (hydrogen alloy, a-Si:H) have also been engineered, via inexpensive *chemical vapour deposition* (CVD) of the junctions, with each pair separated by an *intermediate layer reflector* of Zinc oxide (ZnO) or Silicon oxide (SiO_x) that also enhance light trapping.

To date, there are multi-junction commercial modules on the market made of several combinations of a-Si and micro-crystalline (mc-Si, also referred to as nano-crystalline, nc-Si) junctions, such as: two-junction modules a-Si:H/a-Si:Ge and a-Si:H/mc-Si; three-junction modules a-Si:H/a-Si:H/a-Si:Ge, and a-Si:H/mc-Si/mc-Si. Also “hybrid” structures, depositing a-Si on mono-crystalline Silicon (c-Si) to form a-Si:H/c-Si has recently been studied and developed. Tab. 1 shows the state of the art of various single-, two- and three-junction structures, compared with c-Si and the overall record efficiency non-concentrator cell to date (a 38.8% InGaP/GaAs/InGaAs cell): all values were measured at 1000 W/m², AM1.5g spectrum and 25°C.

Tab. 1: State-of-the-art efficiencies for various single- and multi-junction technologies, compared with the c-Si record device and with the III-V multi-junction record cell. All records refer to 1000 W/m², AM1.5g spectrum and 25°C cell temperature [4-5].

Technology	Junctions	Wavelength range [nm]	Short-circuit current density [mA/cm ²]	Open-circuit voltage [V]	Cell efficiency [%]	Year
a-Si:H	1	300-800	16.75	0.886	10.1	2009
mc-Si	1	300-1200	26.55	0.549	10.7	2012
CdTe	1	300-900	28.59	0.857	19.6	2013
a-Si:H/a-Si:Ge	2	300-900	11.7	1.621	12.5	1992
a-Si:H/ μ c-Si	2	300-1200	12.93	1.365	12.3	2011
a-Si:H/a-Si:H/a-Si:Ge	3	300-900	7.72	2.375	13.5	1996
a-Si:H/ μ c-Si/ μ c-Si	3	300-1200	9.52	1.963	13.4	2012
InGaP/GaAs/InGaAs	3	300-1300	14.27	3.065	38.8*	2013
c-Si (reference)	1	300-1200	42.7	0.706	25.0	1999

*http://www.pv-tech.org/news/spectrolab_surpasses_previous_own_world_record_for_cell_efficiency

Current limitation and spectral mismatch

Because junctions are electrically connected in a series, multi-junction cells and modules face *current-limitation* by the sub-cell that generates the smallest photocurrent. Junction thickness and intermediate-layer reflectors of multi-junction devices can be engineered and optimised so that each junction delivers the same amount of photocurrent, but this is obviously dependent on the spectral irradiance of the incoming light. Furthermore, if a device is designed to have current-matched junctions under a reference spectrum (e.g., the standard AM1.5g) it may face strong *spectral mismatches* in operating conditions under natural variations of the spectral irradiance during the day.

3.3.3 Basics of measurement methods

Current-voltage characterization: reference devices

Because of the multi-junction structure, the choice of reference devices for the detection of total irradiance in current-voltage characterization is particularly challenging and may be discussed under two options:

1. *broadband reference cell* (typically a calibrated c-Si reference cell): this option allows the reference to detect the spectral irradiance over the widest possible wavelength band, where the testing multi-junction device responds;
2. *multiple component reference cells* (typically calibrated, filtered c-Si reference cells [6], while component cells based on thin-film materials are discouraged for stability reasons): this option foresees the usage of a component cell for each junction, in order to detect the fraction of total irradiance that is absorbed by each of the multiple junctions.

The first option may be a good one for open-circuit voltage measurement, because all junctions contribute equally to this parameter due to the series electrical connection [7]; but the spectral mismatch discussed previously usually results in measurements of the short-circuit current affected by strong uncertainties. From this point of view, component cells guarantee that the current-limiting junction receives the appropriate fraction of total irradiance, so that the measured short-circuit is correct.

The choice of the most appropriate reference cell among variously filtered samples can be done, as suggested first in Ref. [8], by selecting the reference cell that shows the same response (or minimal variations) to tiny spectral variations as the testing device. In fact, the use of a perfectly matched reference cell bypasses the calculation of spectral mismatch correction via spectral responsivity measurements, as specified in the following sections 3.4 and 3.5, and may be a practical tool for those labs which cannot perform such measurements.

Because open-circuit voltage measurement is subject to other major uncertainty contributions (thermal and transient effects, above all), using component cells is definitely preferred in the experimental practice; nevertheless, for solar simulators with spectral irradiance that is poorly matched to the standard spectrum, the effect of spectral mismatch on the open-circuit voltage with component reference devices should not be ignored. Furthermore, filters need to be checked carefully and periodically to avoid ageing and subsequent need of recalibration. And, in principle, laboratories involved in the characterization of many different technologies would need a large number of component cells, depending on the growing demand and interest in exotic multi-junction structures, which could be prohibitive. In these cases, even with the best-matched component cell, a spectral mismatch correction is required, as discussed in a dedicated section that follows.

All typical component reference cells show a specific angle of incidence (AOI) behaviour that might be quite different from the regular cosine-behaviour. In this case, the characteristics must be determined by goniometer measurements and need to be incorporated in the measurement uncertainty calculation.

Indoor characterization: requirements for solar simulators

The previous section highlights a key factor in the current-voltage characterization of multi-junction devices: the spectral mismatch between the testing light source and the reference spectrum. This mismatch can easily give rise to huge uncertainties, even with Class A solar simulators in spectral irradiance, i.e., within $\pm 25\%$ spectral match between the simulator's spectral irradiance and the reference spectrum [9] in the following six wavelength bands: 400-500, 500-600, 600-700, 700-800, 800-900, 900-1100 nm, according to IEC 60904-9 [10].

The spectral irradiance matching requirement was introduced when multi-junction devices were not yet developed and is still a valid requirement for first-generation c-Si cells and modules. Discussion is ongoing whether to extend the short wavelength bands to 300 nm for a-Si based devices that respond mainly in the first two of the six wavelength bands above; or even up to 1800 nm, for some germanium-based CPV devices.

Another point under discussion in the PV community is the possibility of introducing a Class A+ requirement, setting a spectral match limit to $\pm 12.5\%$, as has already been suggested by researchers at TÜV Rheinland, Germany [11]. Such a new limit may help to better control the spectral mismatch correction, as specified in section 3.5.

While the American standard for solar simulator requirements ASTM E 927-10 [12] gives the same requirements as the International one, the Japanese standard JIS C 8942 (for which Class A spectral irradiance is reported as Class MA with further restrictions) defines a superior Class MS, for simulators having spectral matching within $\pm 5\%$ [13]. It has to be noted that not only is the matching requirement reduced from $\pm 25\%$ to $\pm 5\%$ for Class MS, but also the

range is extended down to 350 nm and, instead of 6 bands, 15 equidistant bands of 50 nm are defined, which introduces a much stronger requirement than what is defined by either IEC or ASTM.

Spectrally adjustable solar simulators based on multi-lamp systems are a useful option that enables measuring variations of the electrical parameters of the testing module with spectral variations. Also, it may be a very useful option to meet in principle any of the criteria specified in section 3.5 to minimise the spectral mismatch. With a single lamp simulator the intensity of light may be varied in a controlled way, resulting in spectral variations that may be useful for understanding the multi-junction cell's response to changing spectra [14]. This variation is regularly done by changing the current flowing through the lamps or flash tubes together with varying the distance between the source and the testing device to reach optimal balancing conditions.

Above all these topics, the final issue is related to the measurement of spectral irradiance, which is also challenging, especially for pulsed solar simulators. Spectrometers with resolution of 0.5 to 10 nm are available on the market and should be used to measure the spectral irradiance: pulsed solar simulators require very fast-responding instruments, with integration times between 1 and 10 ms. The integration time should be set to allow detection of any variation of spectral irradiance within the duration of data acquisition.

Other important points to be addressed are the transient effects that may result from using short-pulse solar simulators [15]. In fact, certain devices require measurements lasting between 10 and 100 ms or more. Stationary measurements at fixed voltages (the so-called "multiflash procedures") may be introduced to try avoiding these transient effects [16].

Outdoor characterization

Outdoor measurements represent a possible alternative to indoor ones, when the poor spectral irradiance of a solar simulator leads to a large spectral mismatch. In this case, measurements should be performed according to the following requirements:

- AM1.5g spectral irradiance: it can be reached in clear-sky conditions on a tracker and in certain times of the day throughout the year, depending on the geographical location and the period of the year. Various tools may be found online, calculating the air mass as a function of the geographical coordinates and day of the year.
- Cell temperature must be kept close to 25°C over the duration of data acquisition. Temperature coefficients may be determined experimentally [17].
- Broadband reference cells may generally be used in outdoor measurements, because of expected smaller spectral mismatch than in the indoor case; nevertheless, the real spectral irradiance can show non-negligible differences with respect to the standard AM1.5g spectrum. Therefore, the spectral irradiance should be measured and the spectral mismatch should be evaluated as in Ref. [18].

Spectral responsivity

A standard procedure for the spectral responsivity (SR) measurement of multi-junction PV cells and modules is ongoing, based on the standard SR measurement procedure for single-junction devices [19]. With respect to the latter, the following additional requirements need to be followed:

- **supplementary "coloured" bias light:** Bias light is used in single-junction SR measurements in order to put the test device in operating conditions or at least in its range of linear response, when the monochromatic source is not intense enough to do so. In addition, with multi-junction PV devices, bias light is used to avoid current limitation by the junctions that are not being measured; this approach was proposed in the late 1980s and is well-known in the literature [20-21].
- **forward bias voltage:** With supplementary coloured bias light, the production of current from testing a multi-junction device is strongly unbalanced, driving the junction(s) not being tested into forward bias, while the testing junction is reverse-biased. This may lead to an incorrect measurement of the device's SR, in the presence of shunting [22] and should be corrected by applying an appropriate forward bias voltage to the test device.
- **luminescent coupling:** With very high-quality materials a junction in forward bias also experiences radiative coupling, and thus a junction at the top in forward bias, caused by colour bias, may re-radiate light to the testing junction below [23-24]. As a consequence, while measuring middle and bottom junctions some non-zero SR may be measured in the wavelength band of the junction higher in the stack. This contribution does not come from the SR of the testing junction, but as a side effect of luminescent coupling from the junction right above. This effect sometimes increases with increasing intensity of coloured bias light and needs to be treated as a different effect from current-leakage caused by shunting. Recently, certain correction procedures have been suggested in Ref. [25]. This effect is typically a minor one in thin-film modules due to their poor material quality, while it is a dominant one in the high-efficiency III-V multi-junction cells for CPV and space applications.

SR measurements on the testing device may be problematic with large-area modules. It is not trivial to engineer continuous and chopped monochromatic light of commercial module size; the lock-in technique may thus be used while measuring one cell at a time, appropriately light-biasing the entire module and adding the appropriate forward bias (see Ref. [26]). Another option is to use lenses or mirrors to drive and zoom a monochromatic small-size beam to the larger target area [27].

Filtered pulsed simulators are a different option, not involving a lock-in technique, using an instrument that may be already available in PV testing labs, but requiring expensive bandpass filters to cover the full size of the lamp [28]: coloured bias light may again be superimposed on a pulsed monochromatic beam of lower intensities, while additional bias voltage is applied directly to the entire module as mentioned previously, when needed. Fig. 18 shows a schematic of the lock-in technique setup and of the filtered pulsed simulator setup.

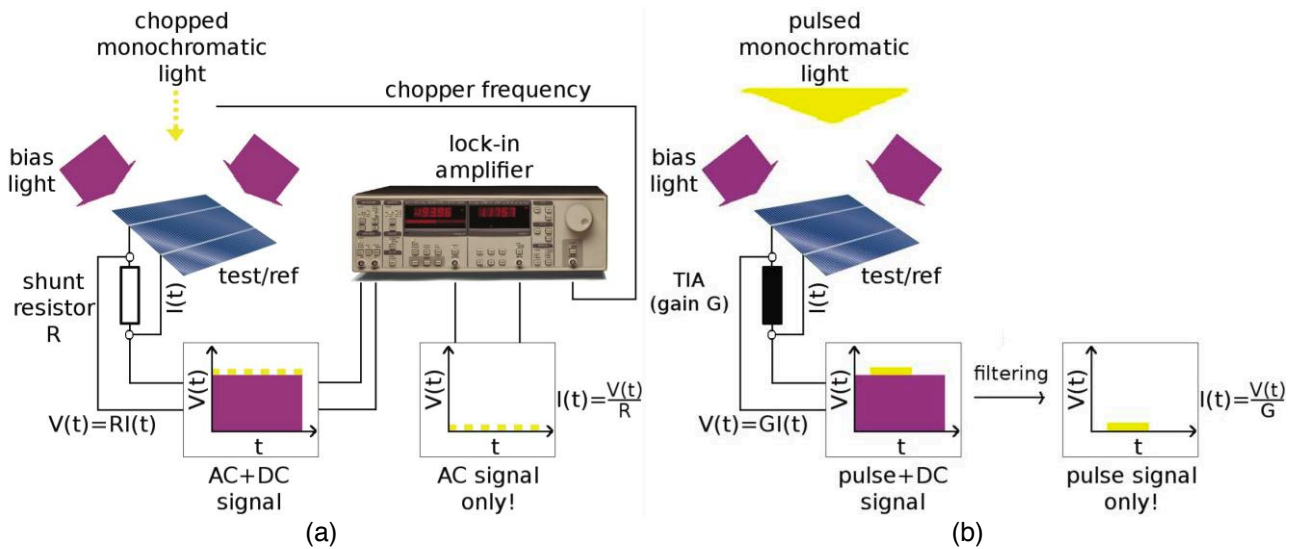


Fig. 18: SR measurement setup, based on: (a) lock-in technique; (b) a filtered pulsed simulator. The shunt resistor may be replaced by a trans-impedance amplifier (TIA) [28].

Spectral mismatch correction

A spectral mismatch correction factor M should be calculated according to IEC 60904-7 [29] for each junction. The factor M_i corresponding to the i -th junction, being current-limiting under given testing spectral conditions, should then be applied to the measured short-circuit current to give the value corrected to AM1.5g. But depending on the choice of the reference detector (see section 3.1) and of the spectral match of the solar simulator in use, M_i may show deviations up to 10% from unity, with huge uncertainties in the final value of short-circuit current. To limit that, it is recommended that researchers use component reference detectors and adjust the spectral irradiance of the solar simulator to lower all M_i deviations from unity below 3%. A limit of 1% would be optimal, but may require a lot of time and effort in spectral adjustment and may not be achievable by all laboratories. Measurement uncertainty should take the M_i into account.

The procedure for spectral tuning (when component reference cells are used and a spectrally adjustable solar simulator is in use) is well described in the ASTM standard E2236-10 [30] and is reported here for simplicity:

1. Adjust the total irradiance of the spectrally adjustable solar simulator to a level close to the desired reporting conditions (1000 W/m^2 for measurements at STC) using a reference cell or previous experience (this initial irradiance level is not critical);
2. Measure the spectral irradiance of the spectrally adjustable solar simulator with a calibrated spectroradiometer;
3. Calculate the spectral mismatch factor M_i for each junction, using the SR of the i -th component reference cell;
4. Measure the short-circuit current of each component reference cell under the spectrally adjustable solar simulator (I_{Ri} , with $i = 1, \dots, N$, being N the number of component cells, equal to the number of junctions);
5. Calculate the *matching factor* Z_i for the i -th junction according to

$$Z_i = \frac{1}{M_i} \frac{I_{sc,i,cal}}{I_{Ri}},$$

where $I_{sc,i,cal}$ is the calibration value of the i -th component reference cell at the reference total spectral irradiance (1000 W/m² at STC).

6. If the matching factor for each component reference cell is within 3%, the spectrally adjustable solar simulator is adjusted to within reasonable limits. If not, increase the spectral content in the appropriate band and repeat steps 2 to 6 until the requirement is met.

A similar method is provided also from the Japanese standard [31]. Z_i and M_i values should be provided in the measurement report, together with the related uncertainties.

Current balance and its effect on the electrical parameters

A further parameter that should be provided in the measurement report is the *current balance* between the i -th and the j -th junction, which is defined as the ratio

$$Bal_{ij} = \frac{J_i}{J_j} = \frac{\int SR_i(\lambda)G(\lambda)d\lambda}{\int SR_j(\lambda)G(\lambda)d\lambda}$$

where J_i is the density of photogenerated current by the i -th junction, having spectral responsivity $SR_i(\lambda)$ and being $G(\lambda)$ the testing spectral irradiance. Bal_{ij} should be calculated for both the incident spectral irradiance and for the reference spectrum and for all pairs of junctions. While the matching factor Z_i gives an indication of the spectral match of the light source in use (with respect to the standard reference), the current balance Bal_{ij} gives an indication of the current match between junctions under the chosen light source.

Of course, Bal_{ij} calculated for the testing light source should be close to the value calculated for the standard reference, being a consequence of good spectral match. Though at the time of this writing there is still no standard target value for it, in line with the requirements of section 3.5 it is recommended that Bal_{ij} under the test spectrum agrees to within at least $\pm 3\%$ with respect to the reference spectrum (optimally $\pm 1\%$, as in the standard for space applications [32]).

All electrical parameters (open-circuit voltage, short-circuit current, fill factor and maximum power) are affected by Bal_{ij} . A plot showing their dependency over current balance should therefore be reported, as in Ref. [33]. A recent survey between different laboratories showed deviations in the maximum power within $\pm 5-8\%$ [34].

3.3.4 Acknowledgments

The authors acknowledge the contributions of Daniela Dirnberger and Holger Seifert at Fraunhofer ISE, Germany; Sarah Kurtz and Keith Emery at the National Renewable Energy Laboratory, United States; Werner Herrmann at TÜV Rheinland, Germany; Yoshihiro Hishikawa at the National Institute of Advanced Industrial Science and Technology (AIST), Japan; Harald Müllejans and Elena Salis at the European Commission, Joint Research Centre, Institute for Energy and Transport, European Solar Test Installation, Italy; Alessandro Virtuani and Gabi Friesen at the University of Applied Sciences and Arts of Southern Switzerland (SUPSI), Switzerland; Johannes Meier at TEL Solar-Lab, Switzerland; Kerstin Keller at TEL Solar, Switzerland and Tom Betts at Loughborough University, United Kingdom.

References for this section

- [1] M. A. Green, Third generation photovoltaics. Advanced solar energy conversion. Springer-Verlag, Berlin, (2003).
- [2] VV. AA., Thin-film silicon solar cells, edited by Arvind Shah, EPFL Press, Lausanne, (2010).
- [3] M. Pravettoni, New Techniques for the Measurement of Second and Third Generation Photovoltaics, Imperial College London, (2011).
- [4] M. A. Green, K. Emery, Y. Hishikawa, W. Warta and E. D. Dunlop, Solar cell efficiency tables (version 42), Prog. Photovolt: Res. Appl. **21**, (2013), pp. 827-837.
- [5] M. A. Green, K. Emery, K. Bucher, D. L. King and S. Igari, Solar Cell Efficiency Tables (Version 9), Prog. Photovolt: Res. Appl. **5**, (1997), pp. 51-54.
- [6] J. Meier, R. Adelhelm, J. Hötzel, D. Romang, S. Bengali and U. Kroll, Reference cells in WPVS Design for precise Micromorph PV power measurements, 25th EU PVSEC / 5th WCPEC, Valencia, (2010), pp. 2728-2734.
- [7] M. Pravettoni, A. Virtuani, K. Keller, M. Apolloni and H. Müllejans, Spectral Mismatch Effect to the Open-circuit Voltage in the Indoor Characterization of Multi-junction Thin-film Photovoltaic Modules, Proc. 39th IEEE PVSC, Tampa, FL, USA, (2013), pp. 0706-0711.
- [8] H. Stiebig, C. Zahren and U. Rau, Simple Approach to Characterise Thin-film Silicon Tandem Cell Modules, Proc. 25th EU PVSEC / 5th WCPEC, Valencia, Spain, (2010), pp. 2744-2747 .
- [9] IEC 60904-3 ed 2.0, Photovoltaic devices - Part 3: Measurement principles for terrestrial photovoltaic (PV) solar devices with reference spectral irradiance data, (2008).
- [10] IEC 60904-9 ed 2.0, Photovoltaic devices - Part 9: Solar simulator performance requirements, (2007).
- [11] W. Herrmann, Uncertainty of solar simulator spectral irradiance data and problems with spectral match classification, Proc. 27th EU PVSEC, Frankfurt, Germany, (2012), pp. 3015 – 3021.
- [12] ASTM E 927-10, Standard Specification for Solar Simulation for Terrestrial Photovoltaic Testing, (2010).
- [13] JIS C 8912:1998/AMENDMENT 1:2005, Solar simulators for crystalline solar cells and modules (Amendment 1), (2005).
- [14] J. Meier, R. Adelhelm, M. Apolloni, K. Keller, Z. Seghrouchni, D. Romang, S. Benagli, U. Kroll, Traceable flasher-based power measurement of MicromorphTM tandem modules, Proc. 26th EU PVSEC, Hamburg, Germany, (2011), pp. 2744-2749.
- [15] A. Virtuani, H. Müllejans and E. D. Dunlop, Comparison of indoor and outdoor performance measurements of recent commercially available solar modules, Prog. Photovolt: Res. Appl. **19**, (2011), pp. 11-20.
- [16] J. Meier, M. Apolloni, K. Keller, R. Adelhelm, D. Romang, S. Benagli, I. Sinicco, Power measurement analysis of MicromorphTM tandem modules, Proc. 28th EU PVSEC, Paris, (2013), pp. 3513 – 3518.
- [17] A. Virtuani, D. Pavanello and G. Friesen, Overview of temperature coefficients of different thin film photovoltaic technologies, Proc. 25th EU PVSEC / 5th WCPEC, Valencia, (2010), pp. 4248 – 4252.
- [18] A. Virtuani, M. Pravettoni and H. Müllejans, Comparison of indoor and outdoor performance measurements on micromorph (a-Si/ μ c-Si) thin-film solar modules, Proc. 23rd EU PVSEC, Valencia, Spain, (2008), pp. 2378-2382.
- [19] IEC 60904-8 ed 2.0, Photovoltaic devices - Part 8: Measurement of spectral response of a photovoltaic (PV) device, (1998).
- [20] J. Burdick and T. Glatfelter, Spectral response and IV measurements of tandem amorphous-silicon alloy solar cells, Solar Cells **18**, (1986), pp. 301-314.
- [21] M. Meusel, C. Baur, G. Létay, A. W. Bett, W. Warta and E. Fernandez, Spectral response measurements of monolithic GaInP/Ga(In)As/Ge triple-junction solar cells: Measurement artifacts and explanation, Prog. Photovolt: Res. Appl. **11**, (2003), pp. 499-514.
- [22] M. Pravettoni, To Bias or Not to Bias? An 'How-To' Guide for Spectral Response Measurements of Thin Film Multi-Junction Photovoltaic Modules, MRS Proceedings **1426**, (2012), pp. 81-86.
- [23] M. A. Steiner and J. F. Geisz Non-linear luminescent coupling in series-connected multijunction solar cells Appl. Phys. Lett. **100**, 251106 (2012), pp. 1-5.
- [24] M. A. Steiner, S. R Kurtz, J. F. Geisz, W. E. McMahon and J. M. Olson Using phase effects to understand measurements of the quantum efficiency and related luminescent coupling in a multijunction solar cell, IEEE Journal of Photovoltaics **2**(4), (2012), pp. 424-433.
- [25] M. A. Steiner, J. F. Geisz, T. E. Moriarty, R. M. France, W. E. McMahon, J. M. Olson, S. R. Kurtz and D. J. Friedman, Measuring IV curves and subcell photocurrents in the presence of luminescent coupling, Journal of Photovoltaics **3**, (2013), pp. 879-887.
- [26] Y. Hishikawa, Y. Tsuno and K. Kurokawa, Spectral response measurements of PV modules and multi-junction devices, Proc. 22nd EU PVSEC, Milan, (2007), pp. 2765-2769.
- [27] M. Pravettoni, A. Komlan, R. Galleano, H. Müllejans and E. D. Dunlop, An alternative method for spectral response measurements of large-area thin-film photovoltaic modules, Prog. Photovolt: Res. Appl. **20**, (2012), pp. 416–422.

- [28] M. Pravettoni, M. Nicola and G. Friesen, A Filtered Pulsed Solar Simulator for Spectral Response Measurements of Multi-junction Modules of Commercial Size, Proc. 27th EU PVSEC, Frankfurt, (2012), pp. 3209-3213.
- [29] IEC 60904-7 ed 3.0, Photovoltaic devices - Part 7: Computation of the spectral mismatch correction for measurements of photovoltaic devices, (2008).
- [30] ASTM E2236-10, Standard Test Method for Measurement of Electrical Performance and Spectral Response of Nonconcentrator Multijunction Photovoltaic Cells and Modules, (2010).
- [31] JIS C 8943:2009, Indoor measuring method of output power for multijunction solar cells and modules (Component reference cell method), (2009).
- [32] ECSS-E-ST-20-08C, European Cooperation for Space Standardization, Space engineering, Photovoltaic assemblies and components, ESA-ESTEC, Noordwijk, Netherland, (31 July 2008).
- [33] M. Meusel, R. Adelhelm, F. Dimroth, A. W. Bett and W. Warta, Spectral mismatch correction and spectrometric characterization of monolithic III-V multi-junction solar cells, Prog. Photovolt: Res. Appl. **10**(4), (2002), pp. 243-255.
- [34] F. Baumgartner, Power rating multi-junction solar cells: Focus Thin Film; Thin Film Industry Forum 2010, Berlin, (April 22nd 2010).

4 Field performance

4.1 Introduction

Thin-film PV modules display a wide variety of behaviours outdoors because of their varied spectral, irradiance and temperature responses and their metastable nature. Predicting the performance of a module based on the conditions outdoors requires an understanding of these effects. This insight can be achieved through a first-principles approach, through empirical models derived solely from measured data, or from a combined strategy.

The following contribution summarises literature concerning the spectral, temperature and transient responses of thin-film PV modules. It is followed by results from a new method of collecting and analyzing data from diverse geographic locations and from multiple PV technologies. Next is a treatment of spectral performance analysis using the average photon energy method on measured spectra, followed by analysis using the average photon wavelength method on simulated spectra.

4.2 Summary of previous studies in the literature

A Louwen and WGJHM van Sark, Utrecht University, Copernicus Institute of Sustainable Development, the Netherlands

4.2.1 Introduction

Standard testing procedures for solar panels prescribe that the power output of panels is rated at standard testing conditions (STC; an overview of standards is given in Ossenbrink et al. [1]). These standard conditions refer to a module temperature of 25°C, 1000 W/m² irradiance and an AM1.5 solar spectrum. Outdoor conditions rarely correspond to these standard values. Therefore, many studies have sought to establish the performance of PV modules under realistic operating conditions, by performing outdoor measurements over longer periods of time.

4.2.2 Spectral effects

Solar cells are rated under spectral conditions according to an air mass of 1.5. However, due to seasonal and intra-day variations of the solar altitude above the horizon, air mass (AM), and thus incident spectrum, show considerable variations. The effect of spectral variations on the performance of crystalline silicon devices is reasonably limited. However, the spectral response of thin-film devices is different from that of crystalline silicon devices, especially for amorphous silicon. Fig. 19 shows the spectral response of thin-film solar cells, compared to several types of crystalline silicon solar cells, as well as the spectrum emitted by a solar simulator (indicated with 'Lapss'). The effect of spectral variations on device performance is measured in different ways in the literature reviewed here. Performance is often expressed in terms of short circuit current I_{sc} or the field-output-factor (FOF), a parameter relating the actual performance to the performance one would expect considering STC efficiency and the irradiance intensity, with corrections for temperature. However, some authors assess performance by showing the useful fraction (UF) of light with varying spectrum. The useful fraction is defined in Ref. [2] as "the ratio of the observed spectral irradiance in the useful

spectral range of the PV device to the observed global irradiance.” Spectral variations are otherwise expressed in either air mass units or average photon energy (APE). Data from a testing facility in Utrecht (UPOT, see Van Sark et al. [3]) has shown APE to decrease with increasing AM unit.

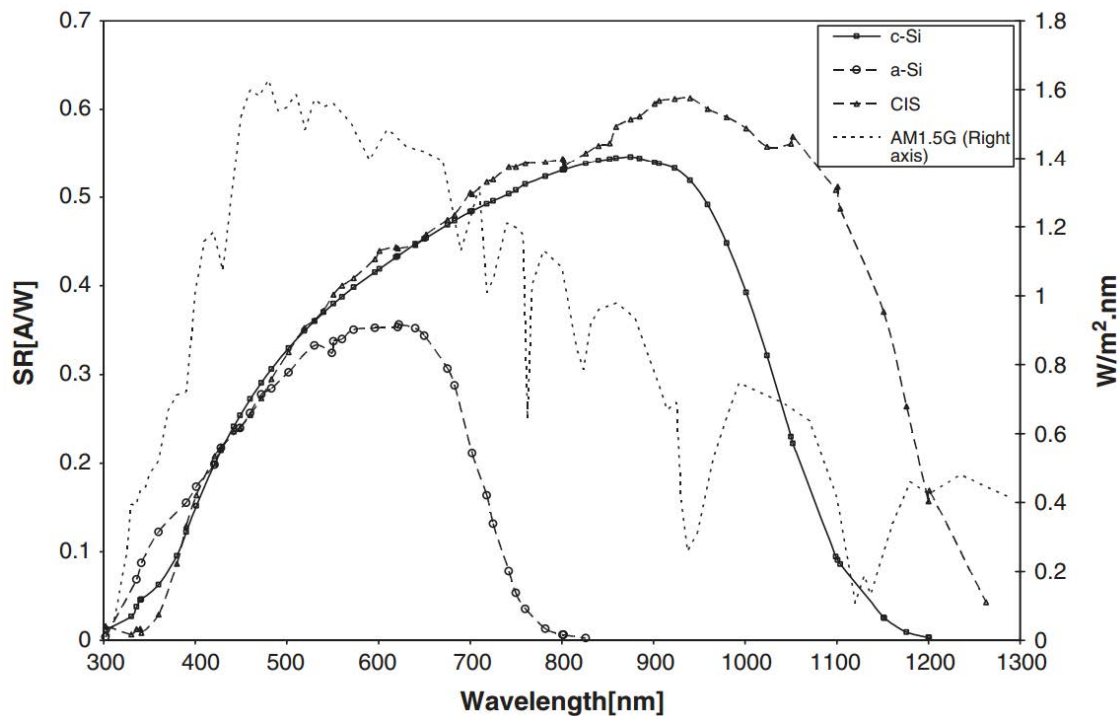


Fig. 19: Spectral response of different module types (CIS, a-Si, c-Si) [4].

Out of the studied thin-film photovoltaic (TFPV) technologies, the effect of spectral variations on performance is most pronounced for amorphous silicon. The approach of researchers in establishing this dependence varies slightly. Some authors have found the performance of a-Si devices, measured in I_{sc} , to decrease with increasing air mass [4–6], and state that this effect is caused by the narrow spectral response of a-Si [4], [5], [7]. This trend is shown in Fig. 20. Fanni et al. [5] furthermore show that the effect of spectral variation is larger for triple-junction a-Si devices compared to single-junction devices, due to current mismatch (see Krishnan et al. [8]). Other authors analyse the spectral dependence of performance based on the FOF and APE and find the FOF to increase with increasing APE [9–11]. Minemoto et al. [10] furthermore establish that APE is indeed a good parameter to analyse the variation of spectrum with a single characteristic measure. Most of the authors mentioned imply a linear response of I_{sc} or FOF to spectral variation (APE or AM). However, we could expect a similar trend as that we see for c-Si: increased performance with increasing APE to a certain maximum performance, after which further increases of APE lead to a decrease in performance. Research correlating FOF to APE shows maximum performance for an APE of about 2 eV, which coincides nicely with the peak in the spectral response of a-Si at about 600 nm. Furthermore the data in Minemoto et al. [10] seem to indicate a decreasing trend after the 2 eV point. However, under normal conditions APEs higher than 2 eV are probably not often measured under higher irradiance conditions that are needed to perform the measurements (in order to exclude low irradiance effects).

The spectral response of CdTe solar cells is less limited compared to a-Si PV, but still somewhat more narrow compared to c-Si devices. Gottschalg et al. [2] have shown the useful

fraction for CdTe devices to vary from +4% to –6% around the annual average. It was also shown that the efficiency of PV modules increases with increasing useful fraction [12].

For CIS/CIGS devices the spectral response is even broader compared to conventional c-Si devices. As expected, this broad response results in spectral variations having the least effect on device performance of the TFPV technologies addressed here. Gottschalg et al. show that for CIS, the useful fraction of the incident light varies by only 5% to 10% during a typical day [2]. Others mention that the effect of spectral variations on CIS performance is small, but quantification of performance change is lacking [4], [13]. Kenny et al. [4] state that the I_{sc} of CIS devices slightly increases with increasing air mass.

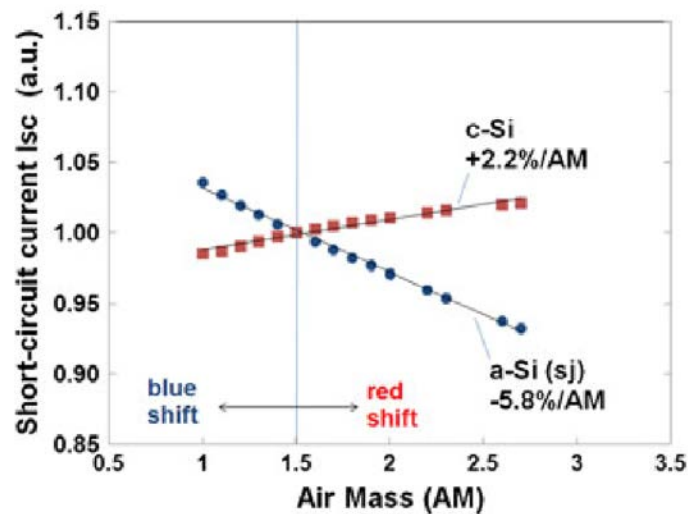


Fig. 20: Modelled dependence of I_{sc} on Air Mass of incident radiation, for single junction a-Si (blue circles) and crystalline silicon (red squares). The dark lines are linear fits to the modeled data points [6].

4.2.3 Temperature effects

The standard test conditions for PV panels refer to a module temperature of 25°C, 1000 W/m² irradiance and an AM1.5 solar spectrum. As we can see from the normal operating cell temperature (NOCT) specified by many PV suppliers, higher module temperatures are easily reached. For most panels, irrespective of technology, the operating temperature of cells at 800 W/m² irradiance, 20°C ambient temperature and a wind speed of 1 ms is about 45°-50°C. For basically all PV technologies, fundamental material physics implies performance loss with increasing operating temperatures. This notion is confirmed by manufacturers with laboratory testing designed specifically to establish temperature coefficients for important operating parameters such as V_{oc} , V_{mp} , I_{sc} , I_{mp} , and, combining those, P_{max} (and thus efficiency). However, to determine if this temperature dependence of performance holds under realistic operating conditions, much research has been performed to test these laboratory-established values.

Makrides et al [14] state that operation at non-STC temperatures results in an average performance loss of 5% for thin-film technologies. Also, it was found that temperature coefficients measured outdoors are generally in accordance with supplier specified data [15]. For amorphous silicon devices, temperature-related performance losses are significant, but much smaller compared to crystalline silicon cells. Of all the thin-film technologies, a-Si is

probably the most studied. Various researchers have found the temperature coefficient of power output to be in the order of $-0.2\%/K$ [5], [15–17]. However, as will be discussed below, because of thermal annealing, higher temperatures can also have positive effects on a-Si performance. CdTe solar cells are generally found to have a slightly larger temperature coefficient, but the effect is still considerably smaller compared to crystalline silicon solar cells at about $-0.25\%/K$ [15], [18]. Temperature coefficients for CIGS devices approach the values commonly observed for c-Si modules. Typically, the temperature coefficient is about $-0.36\%/K$ to $-0.42\%/K$ [15].

4.2.4 Transient and seasonal performance changes

Seasonal variations in TFPV performance result from an interaction of different performance parameters that occur within the same period, but in different phases compared to each other. As is illustrated in Fig. 21, reflection- and spectrum- related losses have a similar timing, due to the relation between angle-of-incidence and air-mass. Temperature effects occur inversely compared to the spectral effects, because it is a general phenomenon that increased temperature leads to decreased performance (excluding the effect of thermal annealing). Various papers were reviewed that specifically assessed the seasonal performance changes of TFPV technologies.

Amorphous silicon

For amorphous silicon modules, seasonal variations are mainly caused by two parameters: temperature and spectrum. Temperature variations lead to changes in performance through two effects on the a-Si devices: decrease of performance due to the negative temperature coefficient and increase of performance due to thermal annealing. As is also shown in Fig. 21, temperature effects would cause a decrease in performance in warmer periods, and an increase in colder periods. Also shown in this figure is the inverse but slightly out-of-phase effect of annealing. Warm temperatures lead to a partial restoration of the degradation that occurs in a-Si devices. Through separation of the effect of different environmental drivers, researchers have shown increasing temperatures to lead to performance decreases in summer because of increased recombination, while performance increases due to thermal annealing effects [5, 6, 14, 19].

Spectral variations lead to performance peaks in summer, because spectra are more favorable (blue-shift) in summer months compared to winter months (red-shift). See also Fig. 20. For a-Si, spectral effects are especially pronounced and various research has confirmed this seasonal spectral effect [5, 12, 15]

Other seasonal effects that are mentioned is the decreased reflectance caused by the lower solar angle in summer [5], although the study by Fanni et al. [5] analysed a horizontally orientated PV installation, which would logically result in increased reflectance in winter compared to tilted installations.

The resulting total seasonal performance is the result of the interplay of these factors. The strength of each seasonal driver on overall seasonal variation seems to be somewhat related to the installed location. Gottschalg et al. [19] and Virtuani et al. [6] state that spectral variations are the main reason for the performance peak observed in summer. Other researchers do find evidence of the influence of spectral changes on seasonal performance, but consider the positive performance effect of thermal annealing the most important driver of

summertime performance peaks [14]. The result is similar however, because the effect of spectrum and annealing overlap and are only slightly out of phase, resulting in performance maxima in summer and minima in winter. This trend is shown in Fig. 21.

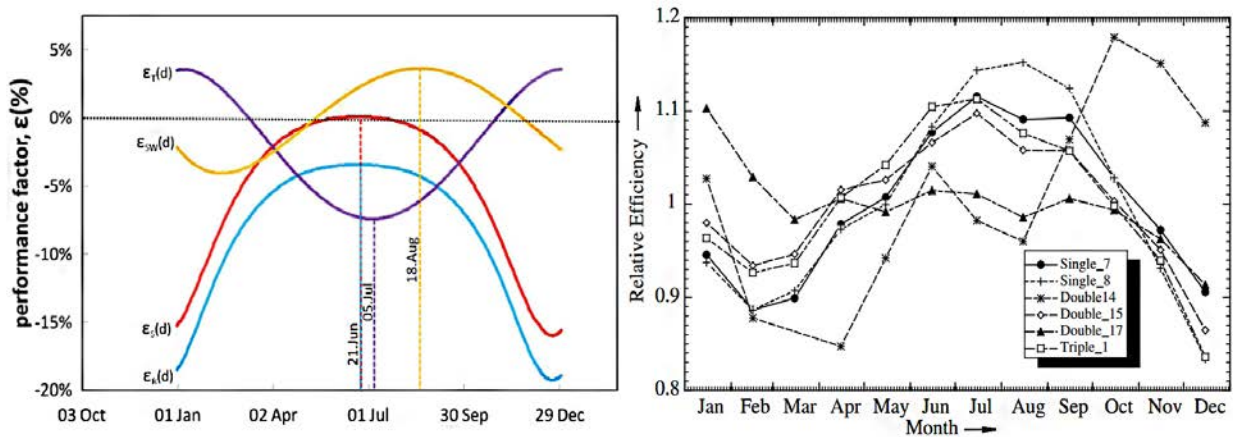


Fig. 21: Left: Overview of the seasonal effects of temperature (ϵ_t), SWE (ϵ_{sw}), reflection (ϵ_r) and spectrum (ϵ_s) on a-Si performance. The effects are expressed as performance factors, the ratio of actual vs. rated performance due to each factor. The total performance factor is obtained by multiplication of the four individual performance factors [5]. Right: Seasonal changes of selected amorphous silicon devices [19].

CdTe and CIGS

For CdTe and CIGS modules, the seasonal performance changes are less pronounced compared to a-Si technology. Because of the limited effect of spectral variation, CIGS modules exhibit seasonal behaviour very comparable to that of c-Si modules. The main factor for CIGS devices is the decrease in summer performance caused by the relatively high dependence of performance on operating temperature [14]. For CdTe, a similar seasonal variation is observed, although the variations are less pronounced because of the lower temperature coefficient [14]. Seasonal performance (monthly DC performance ratio) of CIGS and CdTe modules is shown in Fig. 22.

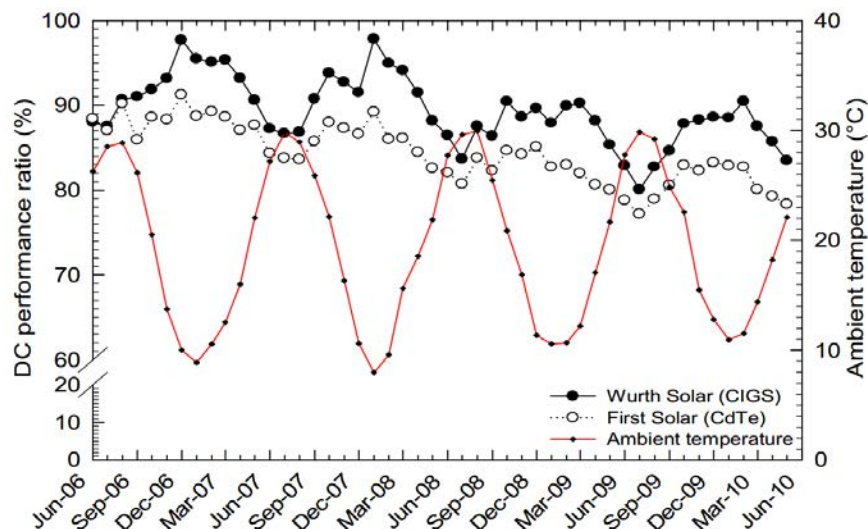


Fig. 22: Monthly average DC performance ratio for thin-film CIGS and CdTe systems over the period June 2006 – June 2010 in Nicosia, Cyprus [14].

References for this section

- [1] H. Ossenbrink, H. Müllejans, R. Kenny, and E. Dunlop, 1.39 - Standards in Photovoltaic Technology, in W.G.J.H.M. van Sark (ed), Photovoltaic Technology Volume 1A in Comprehensive Renewable Energy, A. Sayigh, Ed. Oxford: Elsevier, (2012), pp. 787–803.
- [2] R. Gottschalg, D. G. Infield, and M. J. Kearney, Experimental study of variations of the solar spectrum of relevance to thin-film solar cells, *Solar Energy Materials and Solar Cells*, vol. 79, no. 4, (Sep. 2003), pp. 527–537.
- [3] W. G. J. H. M. van Sark, A. Louwen, A. C. de Waal, B. Elsinga, and R. E. I. . Schropp, UPOT: The Utrecht Photovoltaic Outdoor Test Facility, *Proc. 27th EU PVSEC*, (2012), pp. 3247–3249.
- [4] R.P. Kenny, A. Ioannides, H. Müllejans, W. Zaaiman, E.D. Dunlop, Performance of thin film PV modules, *Thin Solid Films*, Volumes 511–512, (26 July 2006), pp. 663–672.
- [5] L. Fanni, A. Virtuani, and D. Chianese, A detailed analysis of gains and losses of a fully-integrated flat roof amorphous silicon photovoltaic plant, *Solar Energy*, vol. 85, no. 9, (Sep. 2011), pp. 2360–2373.
- [6] A. Virtuani and L. Fanni, Seasonal power fluctuations of amorphous silicon thin-film solar modules: distinguishing between different contributions, *Progress in Photovoltaics: Research and Applications*. doi: 10.1002/pip.2257, (2012), pp. 208–217.
- [7] M. Muñoz-García and O. Marin, Characterization of thin-film PV modules under standard test conditions: Results of indoor and outdoor measurements and the effects of sunlight exposure, *Solar Energy*, vol. 86, no. 10, (Oct. 2012), pp. 3049–3056.
- [8] P. Krishnan, J. W. A. Schüttauf, C. H. M. van der Werf, B. Houshyani Hassanzadeh, W. G. J. H. M. van Sark, and R. E. I. Schropp, Response to simulated typical daily outdoor irradiation conditions of thin-film silicon-based triple-band-gap, triple-junction solar cells, *Solar Energy Materials and Solar Cells*, vol. 93, no. 6–7, (Jun. 2009), pp. 691–697.
- [9] S. Nagae, M. Toda, T. Minemoto, H. Takakura, and Y. Hamakawa, Evaluation of the impact of solar spectrum and temperature variations on output power of silicon-based photovoltaic modules, *Solar Energy Materials and Solar Cells*, vol. 90, no. 20, (Dec. 2006), pp. 3568–3575.
- [10] T. Minemoto, Y. Nakada, H. Takahashi, and H. Takakura, Uniqueness verification of solar spectrum index of average photon energy for evaluating outdoor performance of photovoltaic modules, *Solar Energy*, vol. 83, no. 8, (Aug. 2009), pp. 1294–1299.
- [11] C. Sirisamphanwong and N. Ketjoy, Impact of spectral irradiance distribution on the outdoor performance of photovoltaic system under Thai climatic conditions, *Renewable Energy*, vol. 38, no. 1, (Feb. 2012), pp. 69–74.
- [12] R. Gottschalg and T. Betts, On the importance of considering the incident spectrum when measuring the outdoor performance of amorphous silicon photovoltaic devices, *Measurement Science and Technology*, vol. 15, no. 2, (Feb. 2004), pp. 460–466.
- [13] W. Okullo, M. K. Munji, F. J. Vorster, and E. E. van Dyk, Effects of spectral variation on the device performance of copper indium diselenide and multi-crystalline silicon photovoltaic modules, *Solar Energy Materials and Solar Cells*, vol. 95, no. 2, (Feb. 2011), pp. 759–764.
- [14] G. Makrides, B. Zinsser, A. Phinikarides, M. Schubert, and G. E. Georghiou, Temperature and thermal annealing effects on different photovoltaic technologies, *Renewable Energy*, vol. 43, (Jul. 2012) pp. 407–417.
- [15] G. Makrides, B. Zinsser, G. E. Georghiou, M. Schubert, and J. H. Werner, Temperature behaviour of different photovoltaic systems installed in Cyprus and Germany, *Solar Energy Materials and Solar Cells*, vol. 93, no. 6–7, (Jun. 2009), pp. 1095–1099.
- [16] D. Meneses-Rodríguez, P. P. Horley, J. González-Hernández, Y. V. Vorobiev, and P. N. Gorley, Photovoltaic solar cells performance at elevated temperatures, *Solar energy*, vol. 78, (Feb. 2005), pp. 243–250.
- [17] T. Ishii, K. Otani, and T. Takashima, Effects of solar spectrum and module temperature on outdoor performance of photovoltaic modules in round-robin measurements in Japan, *Progress in Photovoltaics: Research and Applications*, vol. 19, no. 2, (Mar. 2011), pp. 141–148.
- [18] S. Dittmann, W. Durisch, and J. Mayor, Comparison of outdoor and indoor characterization of a CdTe PV module, *Proc. 25th EU PVSEC*, (Sep. 2010), pp. 3508–3512.
- [19] R. Gottschalg, T. Betts, and S. Williams, A critical appraisal of the factors affecting energy production from amorphous silicon photovoltaic arrays in a maritime climate, *Solar energy*, vol. 77, no. 6, (Dec. 2004), pp. 909–916.
- [20] M. Gostein and L. Dunn, Light soaking effects on photovoltaic modules: Overview and literature review, *Proc. 37th IEEE PVSC*, Seattle, WA, USA, (2011), pp. 3126–3131.
- [21] K. Astawa, T. R. Betts, and R. Gottschalg, Effect of loading on long term performance of single junction amorphous silicon modules, *Solar Energy Materials and Solar Cells*, vol. 95, (2011), pp. 119–122.

4.3 Comparison of Different PV Module Technologies: New Method to Analyse Performance Characteristics Obtained from Field Tests at Different Locations

Ulrike Jahn, TÜV Rheinland, Germany

Gabi Friesen, University of Applied Sciences of Southern Switzerland (SUPSI)

4.3.1 Motivation

The energy yield measurements of PV modules at different climatic locations play an important role for the economic operation of PV systems. Assessment of the PV module performance must be investigated under real operating conditions rather than based on data sheet information given by the manufacturer. In recent years, research and industry have developed outdoor test facilities to better understand the climate-dependent performance of PV modules and to gain comparative results of energy yield testing of different technologies. In order to make use of the wealth of available monitoring data in various locations collected by different labs worldwide [1-4], we have undertaken a joint effort to develop a common method to analyse PV module field data obtained from different test facilities and locations.

4.3.2 Approach

Outdoor PV module measurements from seven different locations in Germany, Switzerland, France, Norway, UK, Colorado/USA and Cyprus, are analyzed and compared to demonstrate the new approach. Fig. 23 shows the irradiation profiles and average daylight ambient temperatures of each site. The exposed PV modules from different manufacturers and production years include various thin-film technologies (a-Si, a-Si/ μ -Si, a-Si/a-Si, a-Si/a-Si/a-Si, CIS, CIGS, CdTe) and crystalline Si modules (mono and poly).

The seven outdoor test facilities use different measurement setups (based on MPP tracking or I-V curve tracing), frequency of data recording (10 seconds, 5 minutes, 10 minutes, 15 minutes), cleaning procedures of sensors and modules as well as different periods of outdoor measurements. For this data analysis, the same meteorological parameters are used for the comparison: in-plane irradiance measured by pyranometer G_{pyr} , average ambient temperature T_{amb} and average back-of-module temperature T_{bom} . The $P_{max,STC}$ and $I_{sc,STC}$ values of the PV modules are determined by outdoor or indoor measurements or the nameplate rating is used.

In order to compare the performance characteristics of the modules at the different sites, a common data format was defined (Tab. 2). In a first step, daily performance ratios of P_{max} and of I_{sc} are used as key parameters to characterise the module performance. Spectral data, if available, will be included in a second stage.

More outdoor performance data from labs worldwide is being collected and analysed, while the methods for data evaluation and the result plots for the comparison of different PV module technologies will be further improved.

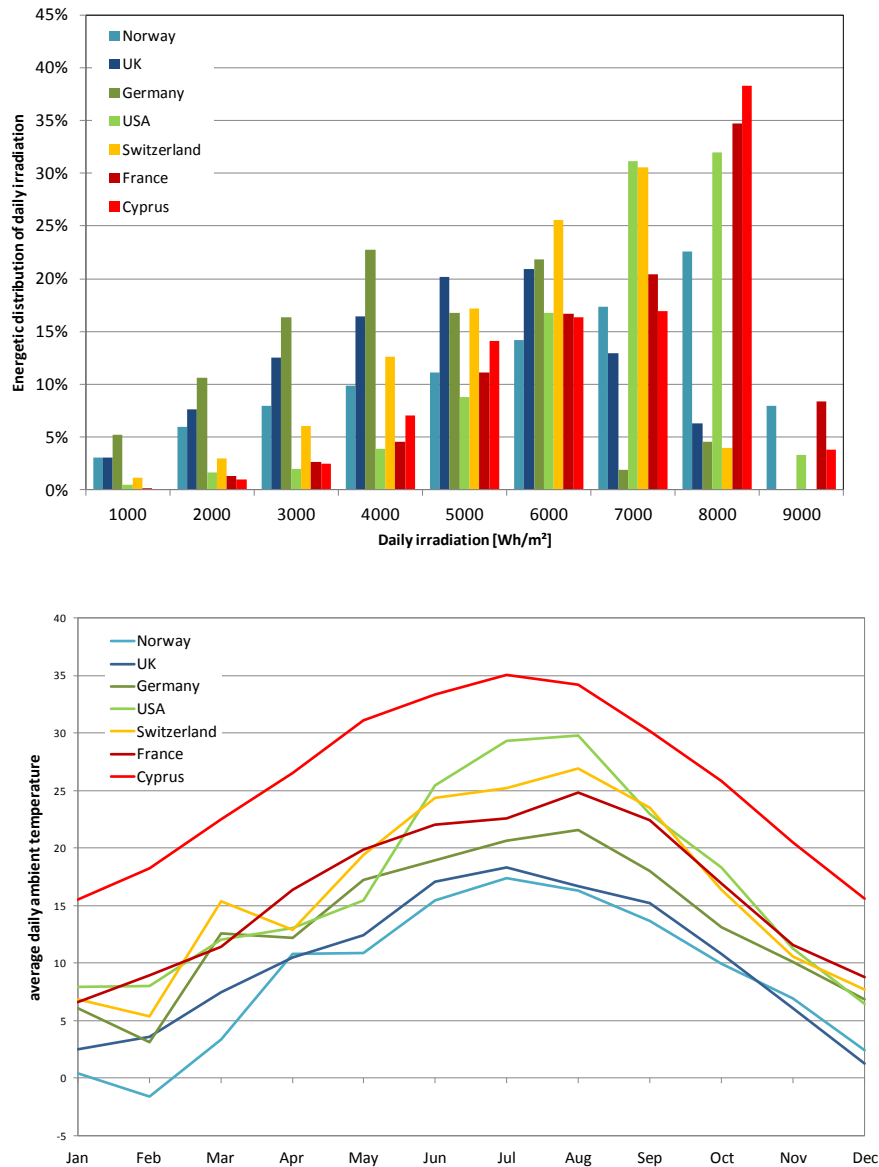


Fig. 23: Meteorological data during monitoring period 2010-2012 at seven different sites. The upper figure shows the different distributions of daily irradiation sums, the lower figure shows the monthly average ambient temperatures measured at the sites.

Tab. 2: Parameters defined and used to perform common data analysis

	Description	Formulas	Condition
Date			
Day type	clear/cloudy/very cloudy		
H_{poa}	daily in-plane (plane of array) irradiation	$\int G_{pyr} dt$	
avg. T_{bom}	daily avg. daylight ($G>0$) back of mod. temp.	$\sum T_{bom}/n$	$G>0$
avg. T_{amb}	daily avg. daylight ($G>0$) air temp.	$\sum T_{amb}/n$	$G>0$
$T_{bom,w}$	daily avg. irr.-weighted module temp.	$\sum T_{bom} \cdot G_{pyr} / \sum G_{pyr}$	$G>0$
PR (Pm)	daily performance ratio of Pmax	$(\sum Pm/Pm, stc) / (\sum G_{pyr}/1000)$	
PR (Isc)	daily performance ratio of Isc	$(\sum Isc/Is, stc) / (\sum G_{pyr}/1000)$	
PR _{filt} (Pm)	daily performance ratio of filtered Pmax	$(\sum Pm/Pm, stc) / (\sum G_{pyr}/1000)$	$G>400W/m^2$ & $AOI<50^\circ$
PR _{filt} (Isc)	daily performance ratio of filtered Isc	$(\sum Isc/Is, stc) / (\sum G_{pyr}/1000)$	$G>400W/m^2$ & $AOI<50^\circ$

4.3.3 Results

The performance ratio $PR(P_{max})$ is the most general performance parameter to characterise PV module and system performance [5]. Fig. 24 shows an example of data representation for some crystalline silicon modules monitored at five different sites.

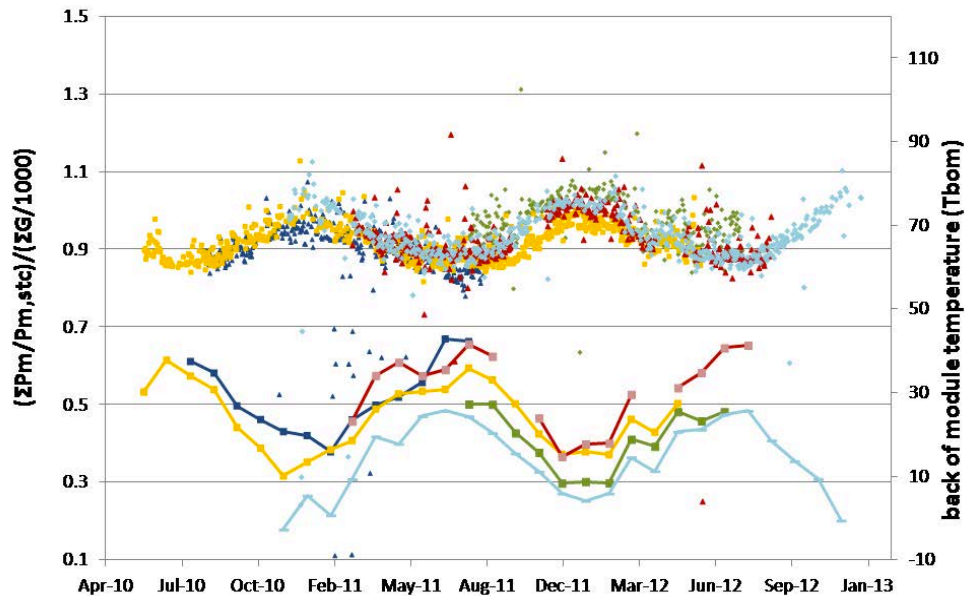


Fig. 24: Average back-of-module temperature for irradiances $G > 0 \text{ W/m}^2$ (line plots) and daily PR for P_{max} (dot plots) for *c-Si* modules at five different sites during monitoring period May 2010 to Dec 2012

Initially, the $PR(P_{max})$ and $PR(I_{sc})$ performance ratio as defined in Tab. 1 are plotted into 1-year plots (if no degradation has been detected over the observed period). Fig. 25 shows the step-by-step approach of how data are analysed. The plots represent different crystalline silicon modules.

Whereas the top/right plot in Fig. 25 shows the typical seasonal variations of $PR(P_{max})$ caused by module temperature, the left plot representing $PR(I_{sc})$ is almost stable because of the very low spectral dependency of c-Si [2]. The $PR(I_{sc})$ variations are in the range of $\pm 5\%$, and they are mainly the sum of the uncertainties in irradiance measurement (pyranometer calibration), determination of I_{sc} at STC and very small spectral variations for c-Si modules. To be able to exclude these uncertainties or influences from further analysis, the first step consists of a correction in which $PR(I_{sc})$ data are set equal to one, followed by application of the so-obtained correction factor to the $PR(P_{max})$ performance ratio. The result of this normalization procedure is shown in plot 3 (middle graph), which then allows analysis of the low-irradiance behaviour in more detail without spectral effects and the pure temperature behaviour as shown in the two lower plots in Fig. 25.

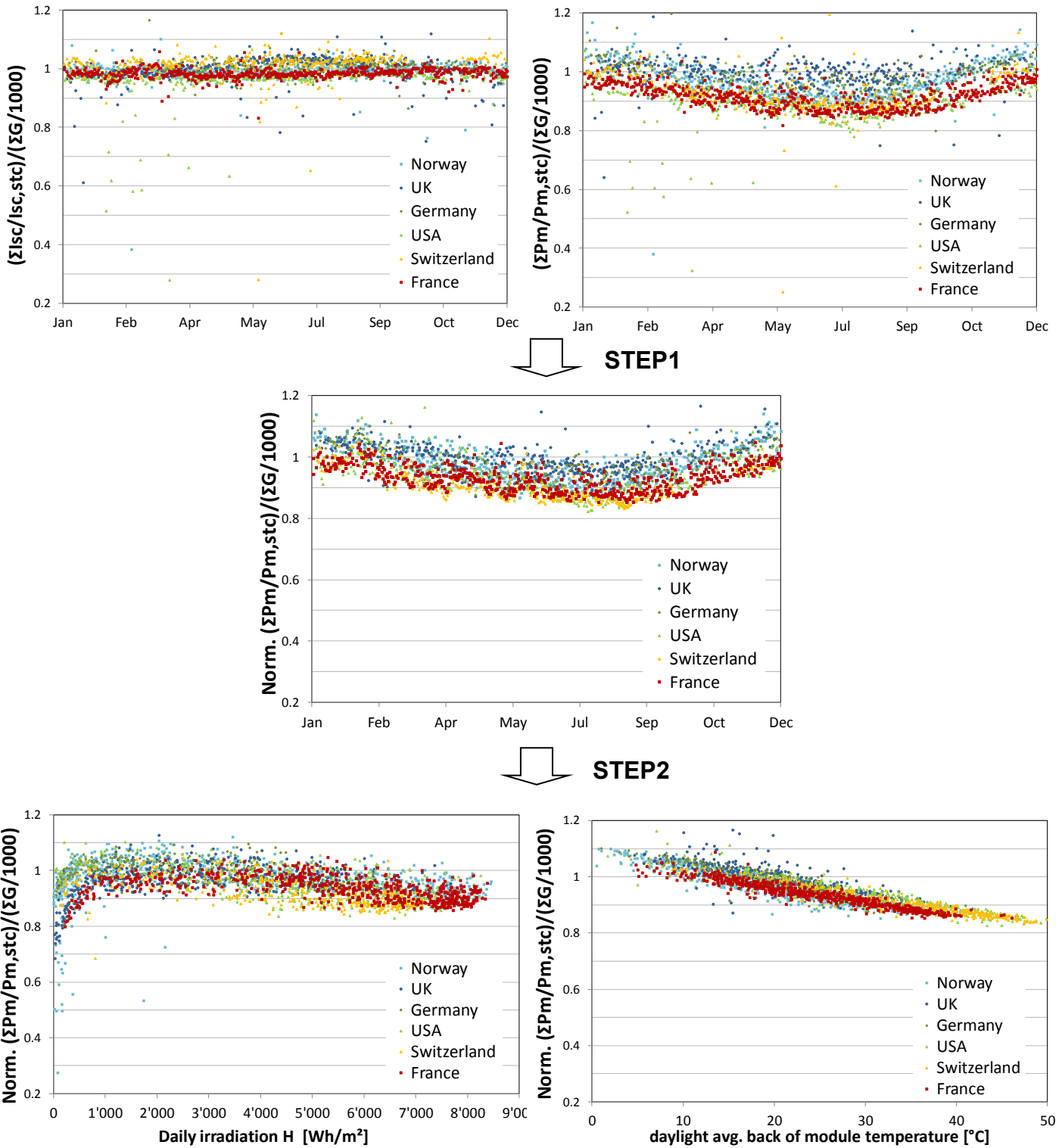


Fig. 25: Example of analysis approach with daily performance ratio $PR(P_{max})$ (top/right) and $PR(I_{sc})$ (top/left) of 6 different *c-Si* modules measured at different locations. Step 1: merge to normalised performance ratio norm. $PR(P_{max})$ and Step 2: plot in dependence of daily irradiation (bottom/left) and of average daylight module temperature (bottom/right).

Fig. 26 shows different amorphous silicon module data (a-Si, a-Si/ μ -Si, a-Si/a-Si, a-Si/a-Si/a-Si) monitored at the seven different sites.

It is well known that amorphous silicon (a-Si) based modules are subject to seasonal variations of performance between 0% to 15% around an average value, which depends on the module technology, local climatic conditions and type of integration [6]. The seasonal variations result from two counteracting effects — light-induced degradation and thermal-induced recovery — also known as the Staebler Wronski effect [7]. The offsets in performance ratio shown in Fig. 26 are caused by the difficulty of determining a unique reference STC power for amorphous silicon. Today no standard approach exists on how to determine a reproducible and unique reference value.

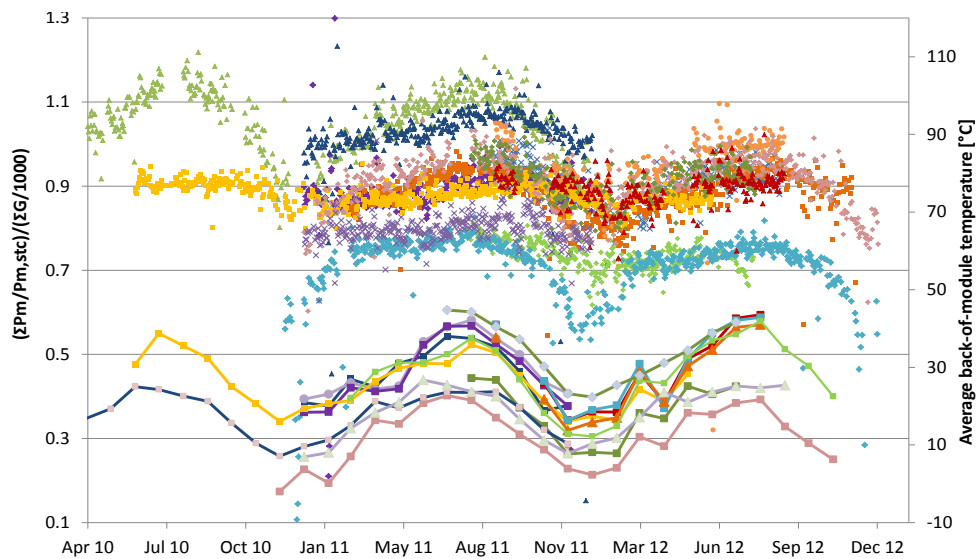


Fig. 26: Average back-of-module temperature for irradiances $G > 0 \text{ W/m}^2$ (line plots) and daily PR of P_{max} (dot plots) for a-Si based modules measured in different locations during monitoring period May 2010 to Dec 2012.

Fig. 27 shows a similar data representation to the c-Si data presented before, now for a selection of 7 different amorphous silicon based modules (1 per location). The first two plots at the top of the figure show how the performance ratio $PR(P_{max})$ and $PR(I_{sc})$ display seasonal variations due to the spectrum, with increasing PR values in summer and decreasing values in winter months. In contrast to c-Si, the Si PV modules display an opposite $PR(P_{max})$ seasonal variation and also show a seasonal variation of the $PR(I_{sc})$ value. The spectrum has a significant impact on both the $PR(P_{max})$ and $PR(I_{sc})$ plots. The normalization step leads to a correction of the spectral effects, and thermal effects are therefore highlighted. The two bottom graphs obtained after the normalization represent the typical low-irradiance and temperature behaviour of amorphous silicon modules.

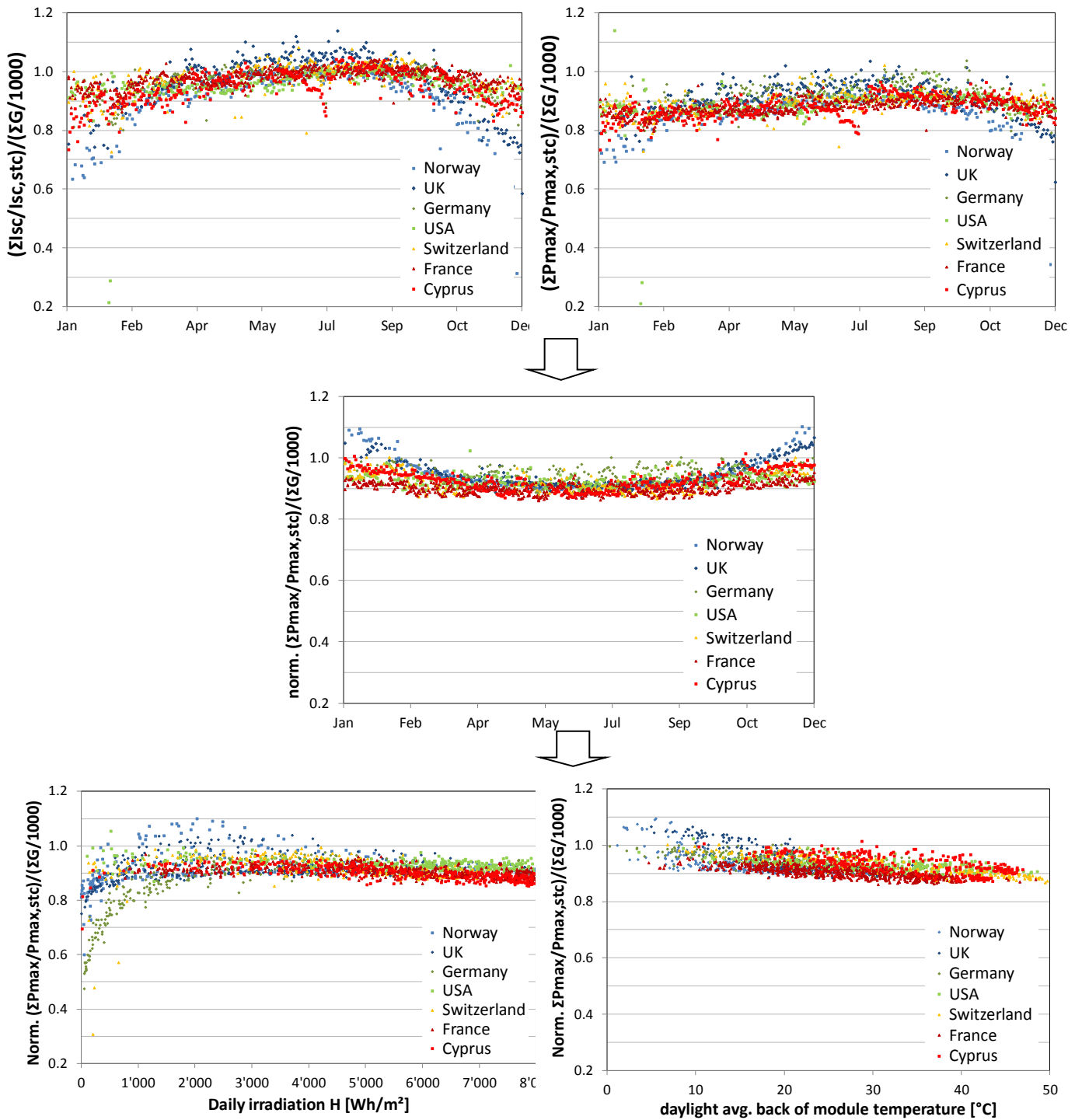


Fig. 27: Example of analysis approach with daily performance ratio $PR(P_{max})$ (top/right) and $PR(I_{sc})$ (top/left) of 7 different *a-Si* based silicon modules measured in different locations. Step 1: merge to normalised performance ratio $norm PR(P_{max})$ and Step 2: plot in dependence of daily irradiation (bottom/left) and of average daylight module temperature (bottom/right).

In contrast to c-Si modules, a-Si PV modules show an opposite $PR(P_{max})$ seasonal variation and a seasonal variation of the $PR(I_{sc})$ value. The spectrum has a significant impact on both plots, the $PR(P_{max})$ and $PR(I_{sc})$. The normalization step leads to a correction of the spectral effects, and thermal effects are thus highlighted. The two bottom graphs obtained after the normalization represent the typical low-irradiance and temperature behaviour of amorphous silicon modules.

References for this section

- [1] G. Friesen. et al., Detailed Analysis of thin-film Module Performance Based on Indoor and Outdoor Tests, Proc. 27th EU PVSEC, Frankfurt, Germany, (2012), pp. 3027 - 3032.
- [2] U. Jahn et al., Final Results of High Precision Indoor and Outdoor Performance Characterization of Various Thin-Film PV Module Technology, Proc. 27th EU PVSEC, Frankfurt, Germany, (2012), pp. 3233–3238.
- [3] J. Merten, et al., Diagnostics of Degradation of thin-films PV Modules During 3.85 Years of Outdoor Exposure, Proc. 27th EU PVSEC, Frankfurt, Germany, (2012), pp. 3219 - 3224.
- [4] Imenes A.G., Yordanov, G.H., Midtgård. O.M., Saetre, T.O. Development of a test station for accurate in situ I-V curve measurements of photovoltaic modules in Southern Norway, 37th IEEE PVSC, Seattle, WA, USA, (2011), pp. 003153-003158.
- [5] IEC 61724, Ed 1.0. Photovoltaic system performance monitoring - Guidelines for measurement, data exchange and analysis. (November 1998).
- [6] L. Fanni et al., A detailed analysis of gains and losses of a fully-integrated flat roof amorphous silicon photovoltaic plant. Solar Energy (2011); 85: pp. 2360–2373.
- [7] Various Authors. Thin-film Silicon Solar Cells. Shah A (ed.), EPFL Press, (2010).

4.4 Analysis of spectral effects on outdoor performance

Markus Schweiger, TÜV Rheinland

4.4.1 Spectral response measurements

The spectral behaviour of PV modules can be described by the external quantum efficiency (EQE). It quantifies the average number of photons per wavelength $\Phi(\lambda)$ which are required for generating one electron by lifting the electron from the valence to the conduction band. The number of electrons is calculated by dividing the current I by the elementary charge q . Taking into account the wavelength dependence of the energy of the different photons, the spectral response (SR) of the device in $\text{AW}^{-1}\text{nm}^{-1}$ can be calculated from the external quantum efficiency. The energy is calculated in terms of the Planck constant h and the frequency f or, inversely, the wavelength λ .

$$QE(\lambda) = \frac{I}{q \cdot \Phi_p(\lambda)} = \frac{SR(\lambda)}{\lambda} \cdot \frac{hc}{q} \quad (1.1)$$

Measurements of the spectral dependencies of the short circuit current I_{sc} differ in measuring with constant photon flux or at constant irradiance. Both methods describe the wavelength intervals in which the cells perform best and are able to generate photocurrent for electrical energy. Generalizing, we can say that the performance in the short-wavelength range depends on the top layers of the module, such as the anti-reflection coating, the glass, the encapsulation material, TCO, the SiO_x layers and upper cell structures. In contrast, the performance at longer wavelengths depends on the lower cell regions and the module temperature. The measurement of the spectral response is important to validate the observed

outdoor spectral behaviour by integrating the solar spectral irradiance with the spectral response.

$$I_{Photo} \approx I_{SC} = A \cdot \int_a^b E_i(\lambda) \cdot SR(\lambda) d\lambda \quad (1.2)$$

Spectral response measurements must be performed according to IEC 60904-8 [3]. Differences between the investigated technologies (CdTe, CIGS, a-Si, a-Si/ μ c-Si, c-Si) as within one technology (a-Si/ μ c-Si, CIGS) have been observed. Representative results are shown in Fig. 28.

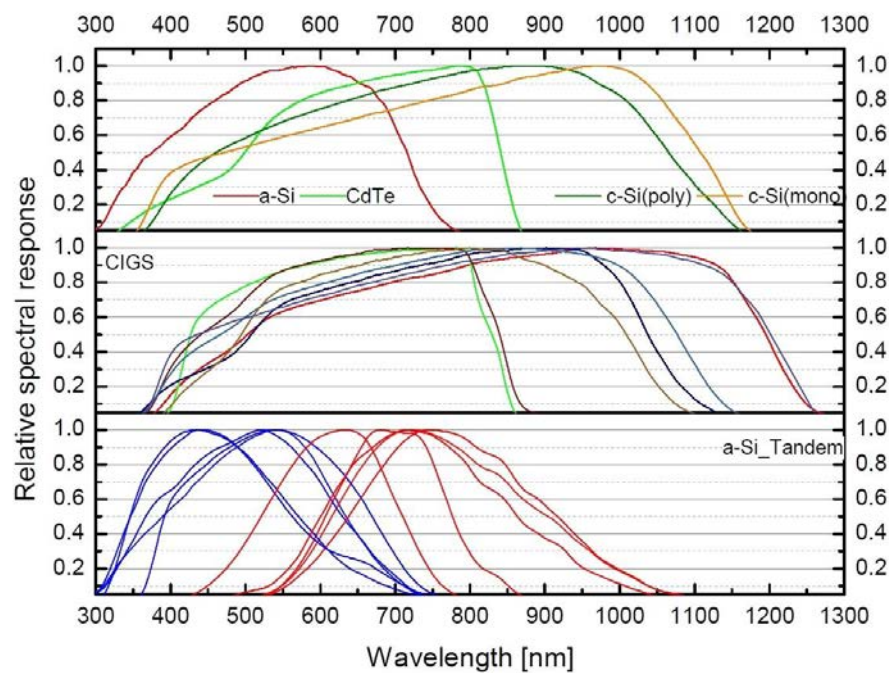


Fig. 28: Relative spectral response signal of different modules, illustrating significant differences within the same thin-film technology

4.4.2 Measuring solar spectral irradiance

For spectral analysis, real solar spectral irradiance data are essential. The spectral conditions in the module plane must be known. These conditions depend on the mounting direction and the location of the test site. Moreover, high data quality is needed. The spectral distribution must be measured fast (<1 s) to reduce the influence of irradiance fluctuations and at least in an interval of (300–1300) nm to be relevant to all technologies, some of which have SR-signals up to 1300 nm (CIGS). Therefore, a combination of a Si-CCD-sensor and an InGaAs-CCD-sensor is needed. Regular calibration of the measurement system at least once a year and a daily cleaning of the input-optics are essential. The input optic and its angle dependency have been identified as one of the crucial factors for spectral measurements, as shown in Fig. 29 and 30.

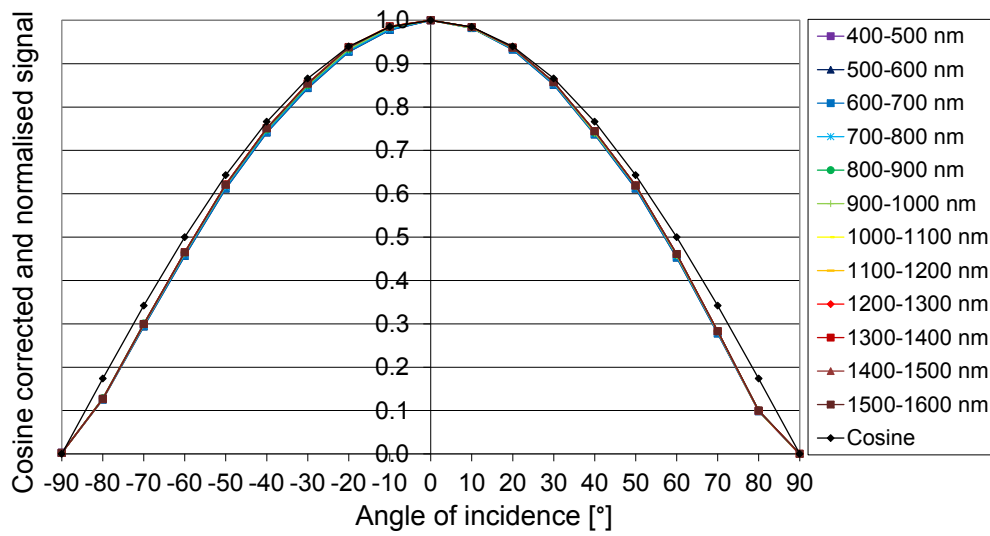


Fig. 29: Angular characteristic of the best performing input optic: spectrally neutral but increasing cosine error above 40°

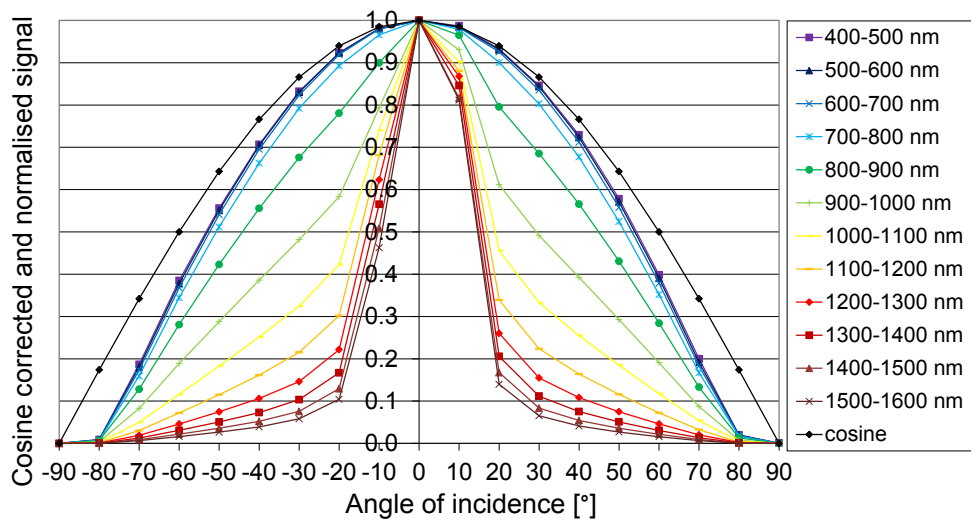


Fig. 30: Angular characteristic of the worst performing input optic: wavelength dependent cosine error

4.4.3 Analysis of large amounts of spectral data with the APE factor

The distribution of the solar spectrum was measured every minute with 1243 data points in the range of (300–1600) nm. The integration time for collecting a complete spectrum was set to about two seconds so as to render fluctuations negligible. During the monitoring period approximately 400,000 spectra were recorded, ruling out manual processing. The raw data spectrum includes the variation in the absolute value of the irradiance, with a maximum at mid-day under blue-sky conditions. The data do not yield qualified information about the blueness or redness of the spectrum suitable for automated data processing. Each spectrum can be classified according to IEC 60904-9 to determine the rough agreement with STC [2] (AM1.5) spectral conditions. This is not an adequate way to analyse shifts in the distribution of the solar spectrum, and the classification is limited to an unsatisfying wavelength interval between 400 and 1100 nm. To evaluate the data from months or years and to describe the blueness or redness of the spectra, the calculation of average photon energy ([APE]=eV) offers an adequate method for simplifying the data and describing a complete spectrum with just a single value [4]. For an integration range of (300–1600) nm, the reference AM1.5 spectrum has an APE value of 1.65 eV. Spectra with an APE < 1.65 eV can be classified as red spectra and spectra with an APE > 1.65 eV as blue.

$$APE = \frac{\int_a^b E_i(\lambda) d\lambda}{q_e' \int_a^b \Phi_i(\lambda) d\lambda} \quad (3.1)$$

where $E_i(\lambda)$ is the spectral irradiance [$W \cdot m^{-2} \cdot nm^{-1}$], the electronic charge q_e' is the conversion factor for obtaining electron-volts instead of joules and $\Phi_i(\lambda)$ is the spectral photon flux density [$m^{-2} \cdot s^{-1}$].

The shapes of the clear-sky APE curves differ for different seasons, as shown in Fig. 31. A strong blue shift in the morning (before approximately 9 am) and evening (after approximately 6 pm) for summer days was observed, due to the sun rising and setting behind the module plane. For winter days the sun rises and sets in front of the module plane. Direct sunlight prevails for nearly the entire winter day and the module must handle large air mass changes over the course of the day. Declining air mass until midday results in a blue shift of the spectrum, reaching a maximum at approximately 12:30 pm. Spectral conditions compliant to the standard can be attained only in spring and fall for modules with fixed mounting. Increasing vapour and aerosol content in the evening was detected only for days with a high air mass. Other mounting directions than south yielded an APE curve shaped similarly to a tangent curve. For cloudy days a strong blue shift in the spectral distribution may be generalised because of the much higher diffuse light fraction. Partly cloudy days show a correlation between the appearance of clouds (low irradiance) and the APE values, as shown in Fig. 32. In characterizing the seasonal conditions, we may generalise and say that the winter months are redder than the summer months, as shown in Fig. 33. This is also the case for diffuse days. The rare clear sky days in winter show a strong red shift. Even in winter diffuse days are very frequent, summer is bluer than winter.

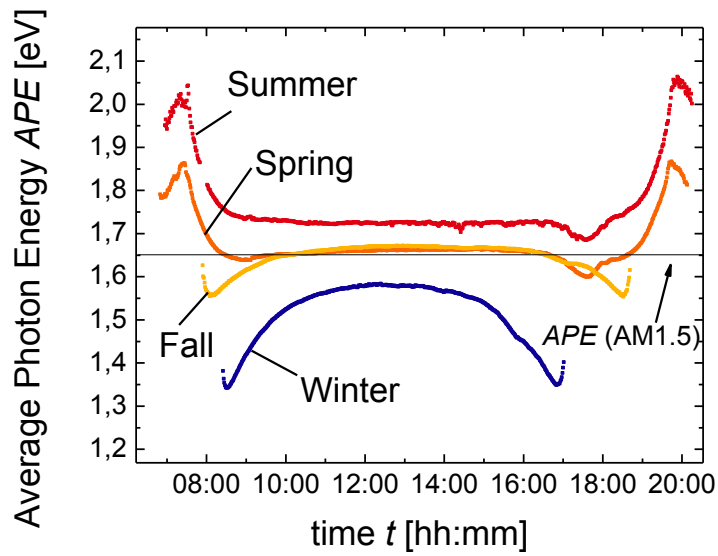


Fig. 31: Solar spectral irradiance drift for four cloudless days in summer (red), spring (orange), all (yellow) and winter (blue), mounted facing south and tilted 35°, in Cologne

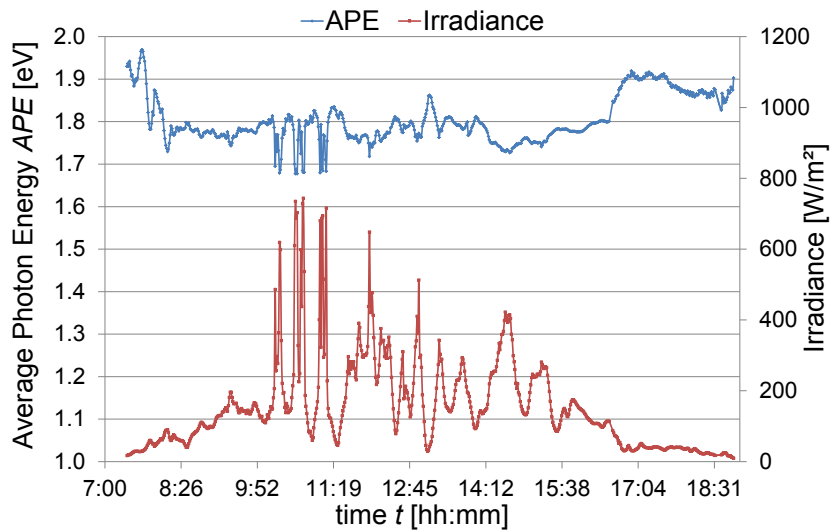


Fig. 32: Characterization of a partly cloudy day (29.08.2010) and correlation of APE values with the appearance of clouds

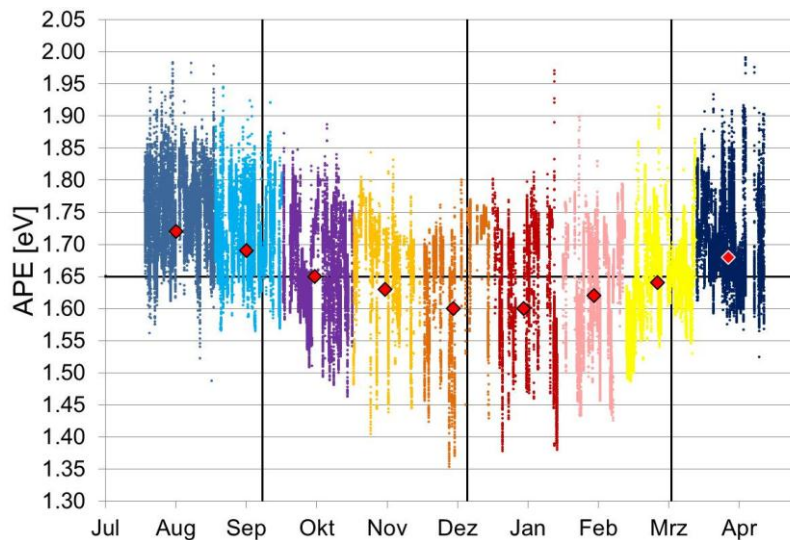


Fig. 33: Seasonal variations of APE values and average APE value per month

4.4.4 Correlating SR data and spectral data with module performance

Shifts in the spectral distribution primarily affect the generated photocurrent. The photocurrent increases linearly with irradiance (as tested and confirmed in the laboratory for all specimens between (100 and 1100) W/m²). If there is a change in the spectrum, the useful fraction for the photo-effect changes. This effect can be offset by a change in the irradiance at the module. Knowing the SR-signals of each module and having measured the real outdoor spectrum, we can calculate the resulting photocurrent theoretically and analyse the current as a function of spectral shifts or rather APE.

To associate this theoretical value of I_{sc} with the measured values of the I-V curves, each curve measured must be corrected for temperature and irradiance relative to comparable conditions (STC). Assuming the I_{sc} is stable during the measurement period and the modules are clean, only the influence of spectral changes remains. The standard IEC 60891 [5] provides appropriate procedures, while procedure No. 2 was selected for this work. Each data point of an I-V curve must be corrected individually with a total of five different parameters. The resulting I_{sc} dependence on spectrum for different module technologies is shown in Fig. 34.

The data should be filtered in order to obtain sharply defined curves of I_{sc} (APE) at least through a plausibility check. When measuring with a pyranometer, data with angles of incidence above 50° must be excluded. Above this angle the good cosine behaviour of the glass dome exceeds the flat module plane, and angle dependence can affect the results. Moreover, possible angle dependences of the SR signal will be locked out, along with the dependence of the SR signal on the irradiance level and temperature. The correction range of the IEC 60891 method should be kept as small as possible and curves at very low irradiation should be discarded because of disturbing influences, such as the strong dependence of the temperature coefficients on the irradiance in some thin-film modules.

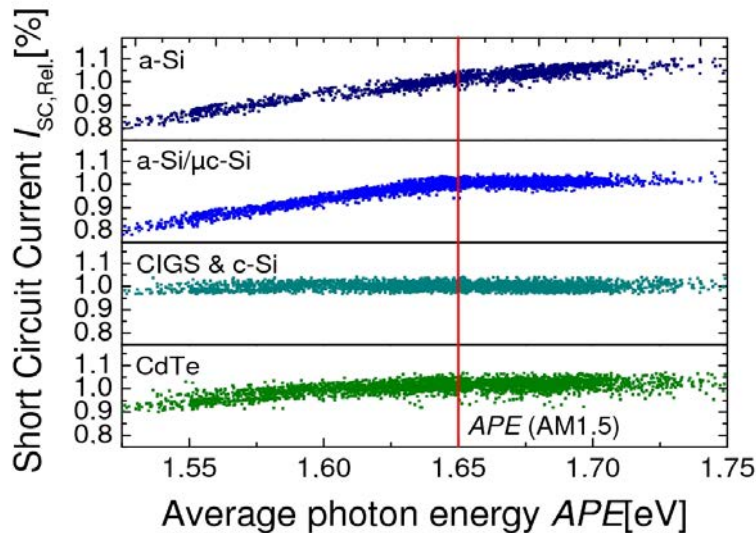


Fig. 34: Dependence of measured I_{sc} on spectral changes (T, G corrected, normalised to I_{sc} , STC (=100%) at 1.65 eV)

4.4.5 Influence of spectral effects on the energy yield of single-junction modules

To characterise the periods of days, months and years, an irradiance-weighted average spectrum was calculated by summing the absolute values of each spectrum and dividing the result by the number of spectra summed over. The correct weighting of each spectrum is obtained by correlating the absolute values with the irradiance at the time of measurement. Assuming that the output power is nearly linear with the short-circuit current, we can quantify the gains or losses in the energy yield. Further weighting with the nonlinear low-irradiance characteristics of P_{max} has not yet occurred at this point.

The annual average spectrum for the analysed test site is shown in Fig. 35. The spectrum nearly fits with the IEC 60904-3 [6] spectrum. The spectral influence for standard crystalline modules is below 1%. Because of the strong dependency of a-Si modules on spectral effects as shown in Fig. 34, gains of up to 3% are possible. Losses caused by spectral effects for the tandem module, because of current mismatch, have to be considered separately.

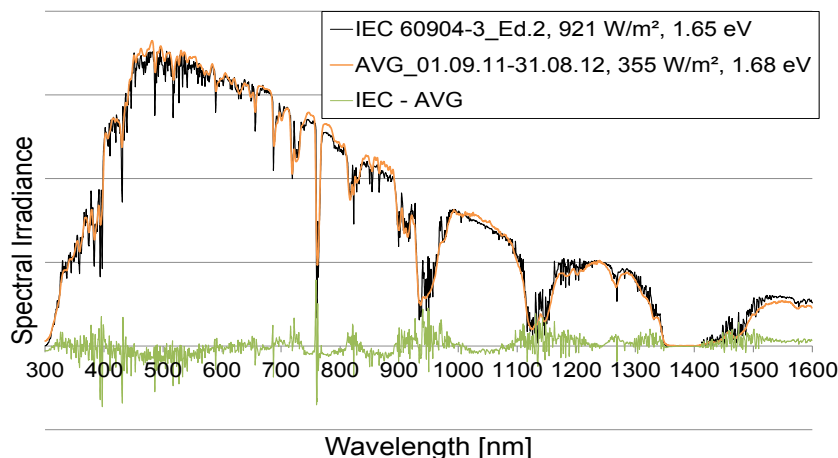


Fig. 35: Average spectrum of the period 01.09.11–31.08.12 relative to AM1.5, area normalised

References for this section

- [1] M. Schweiger et al., Spectral Analysis of Various Thin-Film Modules Using High Precision Spectral Response Data and Solar Spectral Irradiance Data, Proc. 27th EU PVSEC, Frankfurt, Germany, (2012), pp. 3284 – 3290.
- [2] W. Herrmann et al., Uncertainty of Solar Simulator Spectral Irradiance Data and Problems with Spectral Match Classification, Proc. 27th EU PVSEC, Frankfurt, Germany, (2012), pp. 3015 – 3021.
- [3] IEC 60904-8 (CDV), Photovoltaic devices - Part 8: Measurement of spectral response of a photovoltaic (PV) device, (2012).
- [4] T. Betts, Investigation of Photovoltaic Device Operation under Varying Spectral Conditions, Loughborough University, (2004).
- [5] IEC 60891: Photovoltaic devices – Procedures for temperature and irradiance corrections to measured I-V characteristics, (2009-12).
- [6] IEC 60904-3: Photovoltaic devices – Measurement principles for terrestrial photovoltaic (PV) solar devices with reference spectral irradiance data, (2008-03).

4.5 Modeled spectrum method

G. Belluardo, J. Wagner, A. Tetzlaff, P. Ingenhoven, D. Moser (EURAC)

4.5.1 Introduction

Many parameters are used to characterise the quality of spectral distribution: average photon energy [1], air mass [2], useful fraction [3] and spectral mismatch correction [4]. The parameters are based on measured or modeled solar spectra, and may or not require the measurement of the module spectral response.

The purpose of this work is to present the effect of the solar spectrum on the performance of different PV technologies using a methodology that does not require availability of ground measurements of spectral irradiance. The spectral distribution is represented by a unique value, the average wavelength, which is calculated from modeled spectra using satellite-retrieved cloud information. The integral value of spectral distribution is validated through comparison with measured irradiance.

4.5.2 Description of methodology

Modeling of solar spectrum

Spectrally resolved solar surface irradiance is calculated with the SPECMAGIC algorithm [5]. This algorithm produces results with high accuracy and speed because it uses lookup tables (LUTs), i.e., pre-computed radiative transfer model (RTM) results, which contain the transmittance for a variety of atmospheric and surface states. In this way, RTM does not need to be resolved for every satellite pixel and time, but the transmittance can just be extracted from the LUTs by interpolation. Finally, solar surface irradiance can be calculated from the transmittance by multiplication with the extraterrestrial incoming solar flux density.

The following input parameters are taken into account:

- aerosol optical depth (from monthly climatologies)
- surface albedo (using land use maps)
- single scattering albedo (fixed value)
- total column ozone (fixed value)
- water vapor column (from monthly climatologies)
- sun-earth distance

- solar zenith and azimuth angles

In a first stage, the direct and global clear sky spectral irradiance is calculated with the SPECMAGIC algorithm. To decrease the computation run-time the correlated-k approach of Kato et al. is used [6], which divides the whole solar spectrum into 32 bands, each of which is characterised by a unique set of values of gaseous absorption coefficients. The component j of irradiance at generic wavelength λ is derived as follows:

$$I_{j,mod}(\lambda) = I_{j,am1.5}(\lambda) * I_{j,mod}(k) / I_{j,am1.5}(k)$$

Where:

- $I_{j,am1.5}(\lambda)$: irradiance of the standard spectrum at air mass 1.5, at wavelength λ
- $I_{j,mod}(k)$: irradiance modeled with SPECMAGIC, at Kato band k
- $I_{j,am1.5}(k)$: irradiance of the standard spectrum at air mass 1.5, at Kato band k

The direct and global actual spectral irradiance is then obtained by attenuating the clear sky spectral irradiance according to the actual clouds using the cloud index from MeteoSwiss [7]. The cloud index is converted to the clear sky index and direct and global irradiance are simply calculated as the product of clear sky irradiance and clear sky index. A height correction is also performed taking into account the site altitude and solar zenith angle.

The modeled direct and global horizontal spectral irradiance are finally modified in order to take into account the shadowing of the surrounding mountains, and converted to tilted plane by applying a model that assumes an isotropic distribution of diffuse radiation and a fixed value of surface albedo.

Calculation of average wavelength

The average wavelength of a solar spectrum is the wavelength for which the integral value of irradiance at lower wavelengths equals the integral value of irradiance at higher wavelengths. In other words, at the average wavelength the cumulative spectral irradiance is exactly half of the broadband irradiance.

The spectral range considered in this study is between 307 nm and 1965 nm (corresponding to Kato bands 4 to 27). This is done in order to consider the range of photovoltaic conversion of state-of-the-art solar cells (about 300 nm to 1700 nm). The average wavelength values of the AM1.5 standard spectra in the previously mentioned spectral range are 716 nm for direct irradiance and 699 nm for global irradiance.

Measured weather and PV production data

The photovoltaic technologies considered in this study are installed at the Airport Bolzano Dolomiti (ABD) test facility in South Tyrol in northern Italy (46.45778 N, 11.32861 E), which was connected to the medium-voltage grid in August 2010. The plant is composed of a 662 kW commercial section with CdTe modules, and a 62 kW experimental section, with 24 different types of modules, divided into 39 arrays ranging between 1 and 2 kW each, and mounted on fixed racks as well as on single- and dual axis trackers [8]. The technologies considered in this study have a fixed tilt of 30° and an azimuth angle of 8.5° West of South. The site elevation is 262 m above sea level.

The production data are recorded by commercial inverters with a frequency of 15 minutes. The facility is also equipped with a meteo station for the measurement of horizontal (global and diffuse) and global in-plane-with-modules irradiance (secondary standard pyranometers), direct irradiance (secondary standard pyrliometer), and back-of-module temperature (Pt100 sensors).

4.5.3 Results

Validation

The solar irradiance on a horizontal plane and in plane with modules (fixed rack) calculated with SPECMAGIC for the ABD site, considering the whole spectral range, is validated through a comparison with the corresponding measured values, for the year 2011. Fig. 36 and Fig. 37 show a good agreement, both for unfiltered points and for points corresponding to clear sky conditions (ratio of diffuse to global horizontal irradiance lower than 0.20), and for both planes.

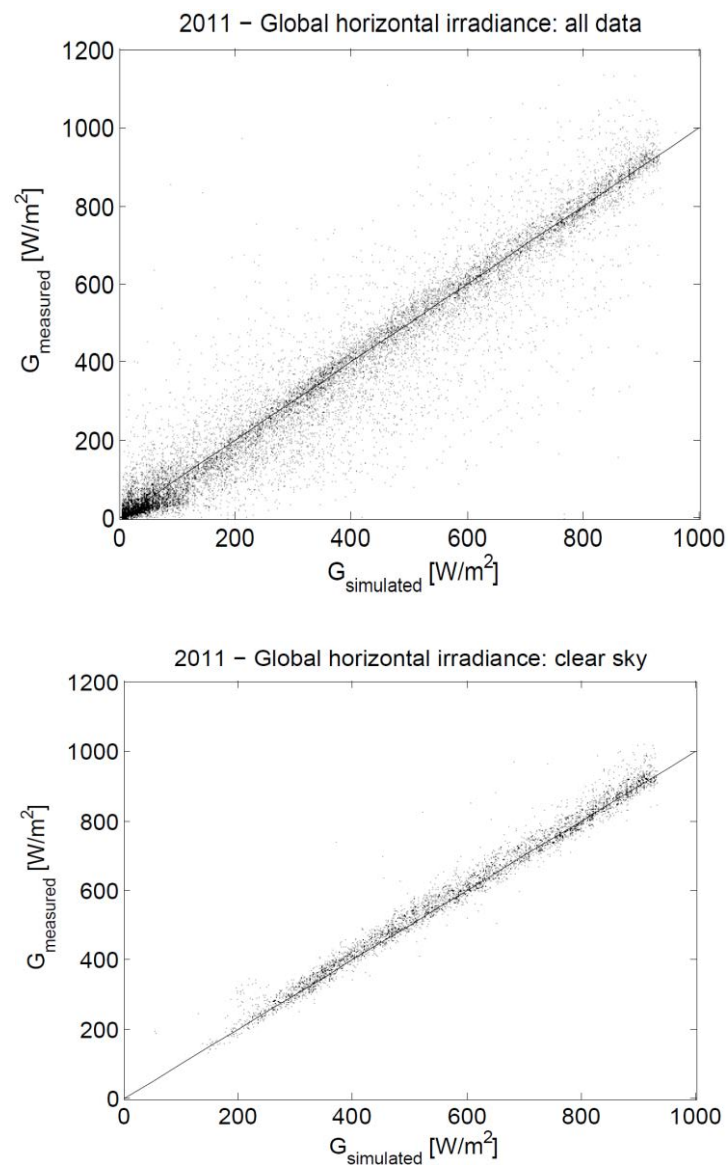


Fig. 36: Comparison of horizontal simulated and measured irradiance for ABD test installation, year 2011. Top: unfiltered points (RMSE=80.2). Bottom: clear sky conditions (RMSE=31.8)

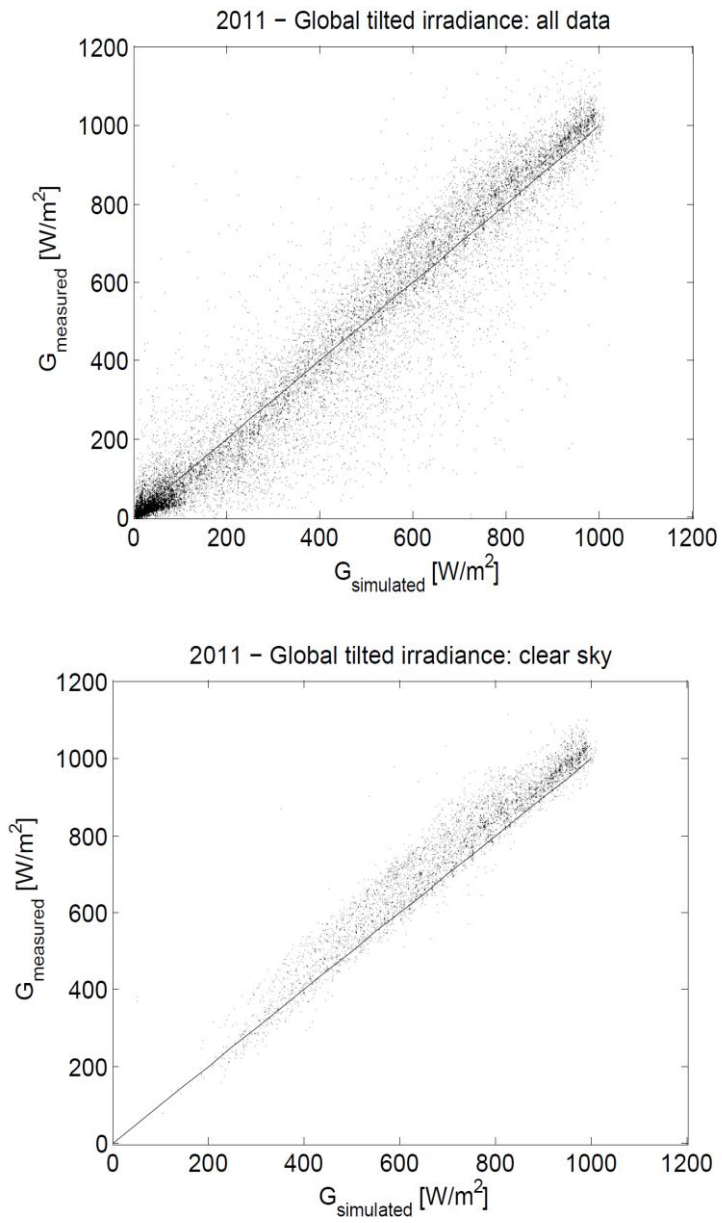


Fig. 37: Comparison of in-plane simulated and measured irradiance for ABD test installation, year 2011. Top: unfiltered points (RMSE=100.870). Bottom: clear sky conditions (RMSE=71.264)

Spectral effects

In this section, relations between modeled average wavelength and PV technology performance are presented for four different thin-film technologies: single-junction amorphous silicon (a-Si), micromorph silicon (a-Si/ μ c-Si), Cadmium Telluride (CdTe) and Copper Indium Gallium Diselenide (CIGS). A polycrystalline silicon technology is also considered as reference.

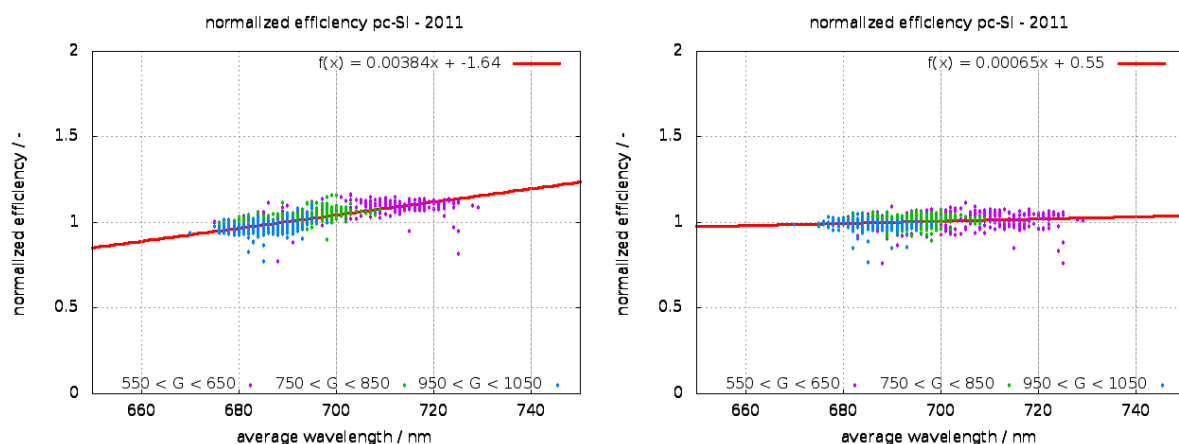
The data here presented are filtered:

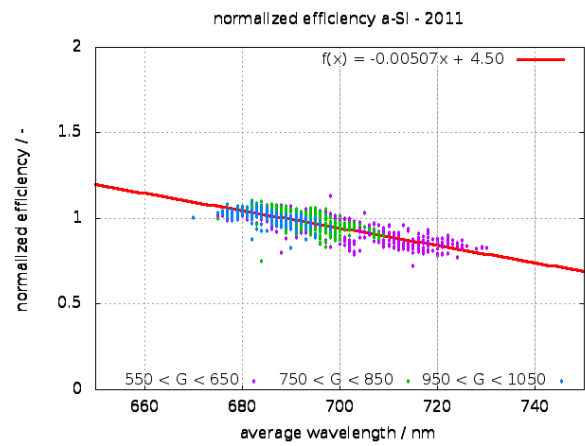
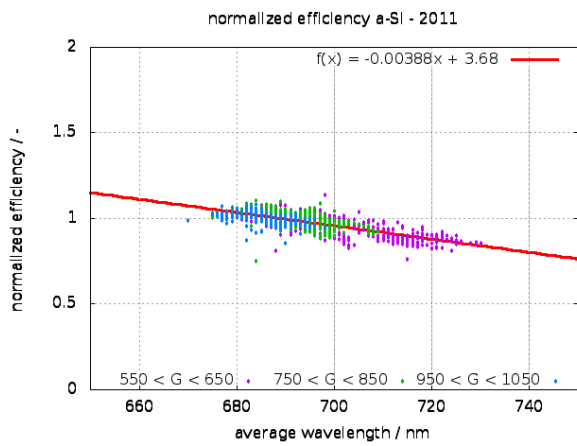
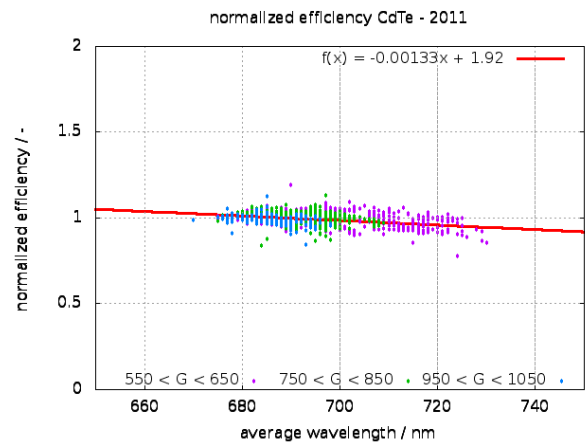
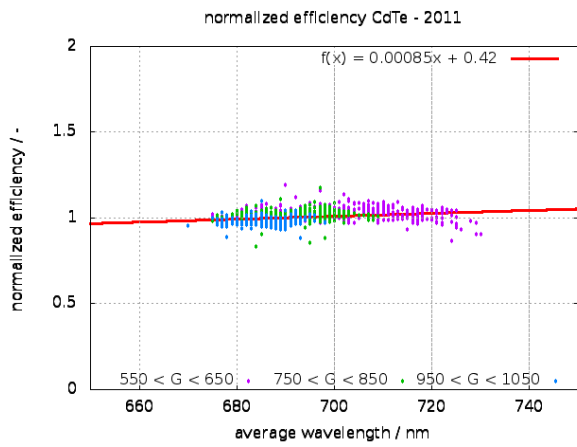
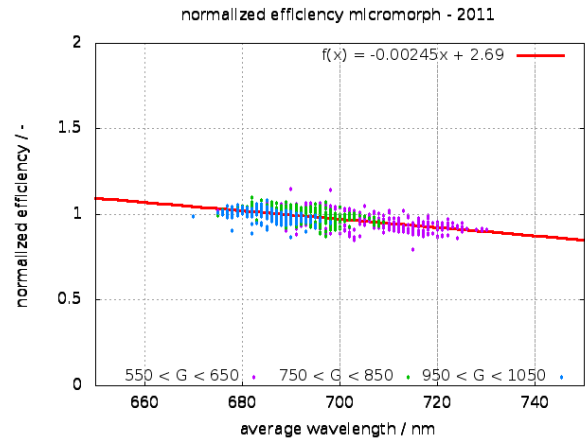
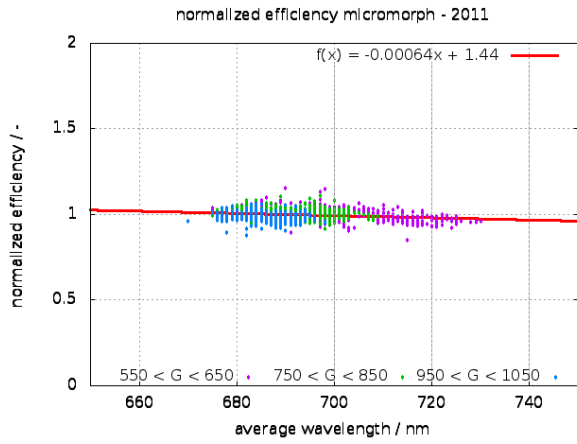
- For Angle Of Incidence (AOI) less than 50° , in order to avoid angle dependence due to mismatch of cosine behaviour of pyranometer glass dome with respect to flat module plane
- Clear sky conditions
- Performance Ratio range given by $PR \pm \sigma PR$ to sort out shadowing effects caused by the mountains and the fact that the plant has only one pyranometer and not one per array.

A temperature correction to 25°C is also performed using temperature coefficients on power from datasheets [9]. Finally, the efficiency is normalised with an efficiency value corresponding to Air Mass 1.5, calculated with a fit on the overall filtered and temperature-corrected points.

In Fig. 38 the normalised efficiency is plotted against modeled average wavelength, for the four thin-film technologies and the reference polycrystalline. Two cases are presented: data filtered (plots on the left) and data filtered and corrected for temperature (plots on the right). Points are grouped per different in-plane irradiance levels, around 600, 800 and 1000 W/m^2 . A linear fit and the corresponding fitting equation is also displayed.

Higher irradiance levels correspond to more “blue-shifted” solar spectra, while lower irradiance levels span a broader range. In any case, irradiance seems not to substantially affect the slope of efficiency cloud.





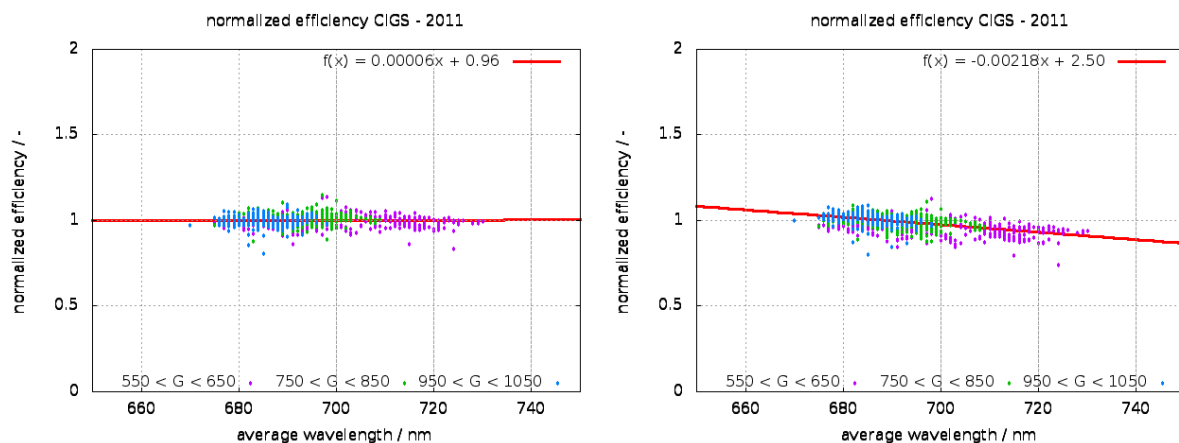


Fig. 38: Normalised efficiency against average wavelength, for clear sky conditions, angle of incidence less than 50°, sorted for shading (left) and filtered and corrected for standard temperature of 25°C (right). Different in-plane irradiance levels are displayed.

The results show that in general the efficiency of thin-film technologies, corrected for temperature, decreases at increasing wavelength of the solar spectrum. This effect is more evident in amorphous-silicon, where it has to be pointed out that the Staebler-Wronski effect plays a certain role. (It has been demonstrated that this effect has a slightly lower influence than spectral effects [3].) Temperature correction is important especially in the case of Cadmium Telluride, where the efficiency trend changes drastically—from increasing with spectrum wavelength to decreasing with spectrum wavelength.

By knowing quantitatively the spectral effects on different technologies it is possible to compare indoor with outdoor data, namely electrical parameters and temperature coefficients.

4.5.4 Acknowledgements

This work was financed through the project "PV Initiative" in cooperation with the autonomous Italian province of Bolzano-Alto Adige, and through the project "PV-Alps", Interreg program IV Italy - Swiss by the European Funds for Regional Development (EFRE).

References for this section

- [1] C. Cornaro, A. Andreotti, Influence of average photon energy index on solar irradiance characteristics and outdoor performance of photovoltaic modules, *Progress in Photovoltaics: Research and Applications*, (2012), pp. 996-1003.
- [2] A. Virtuani, L. Fanni, Seasonal power fluctuations of amorphous silicon thin-film solar modules: distinguishing between different contributions, *Progress in Photovoltaics: Research and Applications*, (2012), pp. 208-217.
- [3] R. Gottschalg, D.G. Infield, M.J. Kearney, Experimental study of variations of the solar spectrum of relevance to thin-film solar cells, *Solar Energy Materials and solar cells*, Volume 79, (Sep. 2003), pp. 527-537.
- [4] B. Marion, Influence of Atmospheric Variations on Photovoltaic Performance and Modeling Their Effects for Days with Clear Skies, 38th IEEE PVSC, Austin, TX, USA, (2012), pp. 003402-003407.
- [5] R. Mueller, T. Behrendt, A. Hammer, A. Kemper, A new algorithm for the satellite-based retrieval of solar surface irradiance in spectral bands, *Remote Sensing*, Volume 4, (Sep. 2012), pp. 622-647.
- [6] S. Kato, T. Ackerman, J. Mather, E. Clothiaux, The k-distribution method and correlated-k approximation for a short-wave radiative transfer, *Journal of Quantitative Spectroscopy and Radiative Transfer*, Volume 62, (1999), pp. 109-121.
- [7] Meteoswiss: CM SAF Data and Methods [Online]. Available at http://meteosuisse.ch/web/en/research/current_projects/climate/cmsaf/data_methods.html[Accessed: 26-Feb-2012].

- [8] G. Belluardo, M. Pichler, D. Moser, M. M. Nikolaeva-Dimitrova, One-year comparison of different thin-film technologies at Bolzano Airport Test Installation. *Fuelling the Future: Advances in Science and Technologies for Energy Generation, Transmission and Storage*, (2012), pp. 229 – 234.
- [9] B. Marion, A methodology for modeling the current-voltage curve of a PV module for outdoor conditions, *Progress in Photovoltaics: Research and Applications*, Vol. 10, (2002), pp. 205-214.

For further information about the IEA – Photovoltaic Power Systems Programme and Task 13 publications, please visit www.iea-pvps.org.



ISBN 978-3-906042-17-6



9 783906 042176 >